J. Fluid Mech. (1975), *vol.* 69, *part* 3, *pp.* 475–511
Printed in Great Britain

The rotating rod viscometer

By G. S. BEAVERS AND D. D. JOSEPH
Department of Aerospace Engineering and Mechanics,
University of Minnesota, Minneapolis

(Received 20 June 1974)

This paper reports the development of practical methods of viscometry to characterize non-Newtonian fluids in slow flow. It is shown that measurements of the free surface near rods rotating in STP and polyacrylamide are accurate, reproducible, and in excellent agreement with a theory of rod climbing. Results are presented that establish the theory and experiment as a viscometer for determining the values of certain (Rivlin–Ericksen) constants that arise in the theory of slow flow. The variation of these constants with temperature in our sample of STP has been explicitly and accurately determined. The experiments in STP show that there is a range of rotational speeds for which STP may be well described by the fluids of grade four. Depth-averaged equations are derived from the equations governing steady axisymmetric flow of any incompressible simple fluid. From the depth-averaged equations, we prove a theorem about the variation of the torque required to turn the rod.

1. Introduction

There is a need in rheology for the development of classes of viscometers that allow investigators to predict the response in slow flow of any rheologically complex fluid whose stress can be expanded into a series of Rivlin–Ericksen tensors. The prediction of the response of this type of fluid requires the determination of the values of certain constants that appear in the coefficients of the expansion (the Rivlin–Ericksen constants). The excellent agreement between theory and experiment demonstrated in this paper and in earlier work indicates that free-surface viscometers, like the rotating rod viscometer, can be used to determine reliable and reproducible values of some of the constants.

In this paper we continue the work of Joseph & Fosdick (1973) and Joseph, Beaves & Fosdick (1973), in which a theory was developed for the Weissenberg effect, and associated experimental data (Joseph *et al.* 1973) were reported. The work described in the above and present papers represents the first stage in a broad programme, aimed at the development of free-surface viscometers.

The *Weissenberg effect* refers to the rise of the free surface in the neighbourhood of a rod rotating in certain non-Newtonian fluids. The rise of the free surface in non-Newtonian fluids is striking, because the free surface sinks when the same rod rotates in Newtonian fluids. Figures 1 (*a*), (*b*) (plate 1) show a rod of 0·476 cm radius rotating at 10 rev s^{-1} in (*a*) a Newtonian oil and (*b*) STP. The free surface rises in STP, but only when the rod radius is below a critical value which depends

exclusively on the material parameters. When the radius is larger than the critical value, then, according to the theory of Joseph *et al.* (1973), the STP will not climp up the rotating rod, as illustrated in figure 1(*c*).

The theory of rod climbing, given in Joseph & Fosdick (1973) and Joseph *et al.* (1973), applies to any rheologically complex fluid whose stress response can be developed around the rest state into a series of stress tensors involving the Rivlin–Ericksen kinematic tensors. The theory gives the shape of the free surface and the motion as a power series in the angular velocity of the rod. In Joseph *et al.* (1973) we achieved good agreement between theory and experiments with STP (a polyisobutylene solution in a petroleum oil base). The comparison between theory and experiments given in Joseph *et al.* (1973) was ambiguous on several points, and left open the question of what agreement could be expected in experiments with fluids other than STP. We call an agreement good when, under all reasonable experimental operating conditions, the comparison of theory and experiment yields unique values for (Rivlin–Ericksen) parameters which in the theory are presumed to be constant at a fixed value of the temperature. In the lowest-order theory, considered in Joseph *et al.* (1973) and here, there is only one constant to determine, the climbing constant $\hat{\beta} = 3\alpha_1 + 2\alpha_2$. In Joseph *et al.* (1973) and here we use two methods for measuring $\hat{\beta}$. We call these *the method of slopes* and *the method of profile fitting*. The methods are described in §6.

Joseph *et al.* (1973) achieved good agreement between theory and experiment using both the method of slopes and the method of profile fitting for several rod radii. But there were apparent discrepancies of the order of 20% in the values obtained for $\hat{\beta}$ with the various rods. These discrepancies appeared to correlate with rod radius, and were much greater than could be attributed to experimental error. Joseph *et al.* (1973) conjectured that the discrepancy might be due to unknown variations in the operating temperature. The experiments reported in this paper, on the variation of $\hat{\beta}$ with temperature, strongly support this conjecture.

In the experiments reported here, we studied the temperature dependence of $\hat{\beta}$ for one sample of STP; we found that

$$\hat{\beta} = 20 \exp(-0{\cdot}115T) \quad (25\ ^\circ\mathrm{C} \leqslant T \leqslant 50\ ^\circ\mathrm{C}). \tag{1.1}$$

We believe that this is probably the first reliable graph of the temperature dependence of a Rivlin–Ericksen constant, other than the viscosity; and it shows that the value of $\hat{\beta}$ is very sensitive to changes in the temperature. For example, the 20% discrepancy in $\hat{\beta}$ noted in Joseph *et al.* (1973) can be explained by a change of temperature of only 2 °C. Temperature changes of more than 2 °C from day to day are common in our laboratory.

The theory and experiment of Joseph *et al.* (1973) were imperfectly matched. The theory presumed that the free surface of the fluid (STP) was perpendicular to the rod surface; the experiments had quite large wetting angles. To correct for the static rise due to wetting, we added, to the rise computed from theory, a rise due to wetting computed from the surface-tension equation, with the value of the prescribed contact angle taken from experiments. In the new experiments

we were able to achieve the flat contact assumed in the theory, by coating the rod with 'Scotchgard'.†

To test the theory on a second fluid, we studied the climb near rods which rotate in polyacrylamide solutions. As in STP, the rise is linear in the square of the angular velocity over an interval which is sufficiently large to make easy the comparison of results from second-order theory with experiment. We regard the presence of large regions of linearity in the height rise curves as a stroke of good luck. The curvature of the height rise curve at the origin could be appreciable; in fact, the absence of measurable curvature near the origin, which holds for STP at all temperatures in the range investigated and for polyacrylamide near room temperatures, does not hold for polyacrylamide at elevated temperatures.

We are continuing this study of the rotating rod viscometer by inclusion of the higher-order theory, which gives the curvature of the rise curve at the origin. The higher-order theory is needed for materials that do not have a nearly linear rise curve at the origin. For 'good' materials with linear rise curves, like STP, the higher-order theory should lead to the determination of values of the higher-order Rivlin–Ericksen constants, which have never been measured. The results of experiments reported here indicate that it might be possible to determine higher-order Rivlin–Ericksen constants for STP (see figure 17).

The analysis presented in this paper includes a derivation of depth-averaged equations. These arise when the governing equations for steady axisymmetric motions of a simple fluid, in general form, are averaged with respect to depth. The resulting equations are exact statements, without approximations, in integral form, of the conservation of momentum on cylinders drawn in the fluid around the rod. They have some promise for approximate and Galerkin analysis. From one of these equations, we derive an interesting theorem about the variation of the torque required to turn the rod.

2. Viscometry for simple fluids

Newcomers to the study of the fluid dynamics of rheologically complex fluids are surprised that it is necessary to maintain a distinction between constitutive relations that apply to one and the same fluid undergoing different types of motion. The stresses in a rheologically complex fluid depend on the history of the deformation, and may take on entirely different forms when the histories are different. One and the same material may actually appear to satisfy different constitutive equations when undergoing different types of motion.

One mathematical theory, general enough to characterize the stress response of a single fluid in different types of flow, has been given by Noll (1958). In Noll's theory (see Truesdell & Noll 1965), the rheologically complex fluid is called simple, and its stress is determined by the history of the deformation gradient

† 'Scotchgard' is a brand name for a commercial waterproofing agent, mainly used on fabrics. It is manufactured by the 3-M Company. We are indebted to L. E. Scriven for suggesting that we coat the rods with Scotchgard.

For flows in which the density ρ of the fluid is constant, the stress $\mathbf{T}$ is equal to an isotropic part, the 'pressure' $-p\mathbf{1}$, plus the extra stress:

$$\mathbf{S} = \mathscr{F}[\nabla\boldsymbol{\xi}^T\nabla\boldsymbol{\xi} - \mathbf{1}] = \mathbf{T} + p\mathbf{1}. \tag{2.1}$$

$\boldsymbol{\xi} = \boldsymbol{\chi}_t(\mathbf{x}, \tau)$ is the position at time $\tau \leqslant t$ of a particle which at the present time t is at the point $\boldsymbol{\xi} = \mathbf{x}$.

The problem of viscometry for simple fluids, generally stated, is to find the form of the operator $\mathscr{F}$ for a given fluid. This is an extremely hard problem, and its solution is unknown, except for the tremendously important case of a Navier–Stokes fluid.

To circumvent the difficulty of doing practical fluid mechanics with a general but unknown $\mathscr{F}$, it is useful to define restricted problems of viscometry. These take form by first specifying classes of motion or histories on which $\mathscr{F}$ reduces to something more manageable, then defining viscometry relative to the more manageable $\mathscr{F}$. For example, on small-amplitude motions of arbitrary frequency, $\mathscr{F}$ reduces to the constitutive equation of linear viscoelasticity. Here the fluid is completely characterized by a shear relaxation modulus (Coleman & Noll 1961; Markovitz & Coleman 1964). The goal of viscometry for simple fluids in small-amplitude motions of arbitrary frequency is to find the form of the shear relaxation modulus.

A different problem of viscometry is associated with viscometric flows. Such flows are locally equivalent to pure shearing as in Couette flow or Poiseuille flow. For viscometric flows $\mathscr{F}$ reduces to three scalar functions of the rate of shearing (see Coleman, Markovitz & Noll 1966). Nearly all of the existing viscometers are based on viscometric flow theory and lead to graphs of the three scalar functions. The response $\mathscr{F}$ for some single fluid in all viscometric flows is known when the three scalar functions are known; but knowing the three functions does not suffice to describe $\mathscr{F}$ in motions more general than viscometric. It is, therefore, possible in principle to predict the response of a simple fluid in Couette flow from experiments, say, on Poiseuille flow but these experiments would not suffice to describe flow around a sphere, or between rotating spheres, or in a Couette apparatus with ends.

Yet another problem of viscometry is associated with a class of simple fluids in smooth slow steady motions. We call $\mathbf{U}(\mathbf{x}, \epsilon) = \epsilon\mathbf{u}(\mathbf{x}, \epsilon)$ a smooth steady motion if $\mathbf{u}(\mathbf{x}, 0)$ and all of its spatial derivatives are continuous and uniformly bounded in the closure of the domain on which they are defined. Assuming that $\mathscr{F}$ is expandable† on steady histories such that $\mathbf{U} = \epsilon\mathbf{u}(\mathbf{x})$, $\mathscr{F}$ may be expanded into a Taylor series, whose partial sum is

$$\mathbf{S}_{(N)} = \sum_1^N \mathbf{S}_n[\mathbf{A}_n, \mathbf{A}_{n-1}, \ldots, \mathbf{A}_1] = \sum_1^N \epsilon^n \mathbf{S}_n[\mathbf{a}_n, \mathbf{a}_{n-1}, \ldots].$$

† Coleman & Noll (1960) were the first to write down these expansions; they also gave sufficient (but not necessary) conditions for convergence. Their expansion uses a retardation parameter α which leads to a slow time αt. Their forms for the $\mathbf{S}_n$ reduce to the ones used here when time derivatives are set to zero. For steady flows, the correct forms of the expansions also follow from setting $\mathbf{U} = \epsilon\mathbf{u}$ in the stress tensors for the Rivlin–Ericksen fluids (Giesekus 1961; Langlois & Rivlin 1963).

$\mathbf{A}_n = \epsilon^n \mathbf{a}_n$; the $\mathbf{A}_n$ are Rivlin–Ericksen kinematic tensors defined by

$$(\mathbf{A}_1)_{ij} = \frac{\partial U_i}{\partial x_j} + \frac{\partial U_j}{\partial x_i}$$

and

$$(\mathbf{A}_{n+1})_{ij} = U_l \frac{\partial}{\partial x_l}(\mathbf{A}_n)_{ij} + (\mathbf{A}_n)_{il}\frac{\partial U_l}{\partial x_j} + (\mathbf{A}_n)_{jl}\frac{\partial U_l}{\partial x_i}.$$

The first four of the tensors $\mathbf{S}_n$ are

$$\begin{aligned}
&\mathbf{S}_1[\mathbf{A}_1] = \mu \mathbf{A}_1,\\
&\mathbf{S}_2[\mathbf{A}_1, \mathbf{A}_2] = \alpha_1 \mathbf{A}_2 + \alpha_2 \mathbf{A}_1^2,\\
&\mathbf{S}_3[\mathbf{A}_1, \mathbf{A}_2, \mathbf{A}_3] = \beta_1 \mathbf{A}_3 + \beta_2(\mathbf{A}_2\mathbf{A}_1 + \mathbf{A}_1\mathbf{A}_2) + \beta_3(\operatorname{tr}\mathbf{A}_2)\,\mathbf{A}_1,\\
&\mathbf{S}_4[\mathbf{A}_1, \mathbf{A}_2, \mathbf{A}_3, \mathbf{A}_4] = \gamma_1 \mathbf{A}_4 + \gamma_2(\mathbf{A}_3\mathbf{A}_1 + \mathbf{A}_1\mathbf{A}_3) + \gamma_3 \mathbf{A}_2^2\\
&\qquad + \gamma_4(\mathbf{A}_2\mathbf{A}_1^2 + \mathbf{A}_1^2\mathbf{A}_2) + \gamma_5(\operatorname{tr}\mathbf{A}_2)\,\mathbf{A}_2 + \gamma_6(\operatorname{tr}\mathbf{A}_2)\,\mathbf{A}_1^2\\
&\qquad + [\gamma_7 \operatorname{tr}\mathbf{A}_3 + \gamma_8(\operatorname{tr}\mathbf{A}_1\mathbf{A}_2)]\,\mathbf{A}_1. \qquad (2.2)
\end{aligned}$$

The coefficients $\mu, \alpha_1, \alpha_2, \beta_1, \beta_2, \beta_3, \gamma_1, \gamma_2, \ldots, \gamma_8$ are (Rivlin–Ericksen) constants, or, more generally, functions of the temperature.†

The Rivlin–Ericksen kinematic tensors and the tensors $\mathbf{S}_n$ are homogeneous and of degree n in the derivatives of $\mathbf{U}$. In perturbation studies, it is convenient to call attention to the fact that the $\mathbf{S}_n$ are homogeneous polynomials in $\mathbf{U}$. For this reason, we define the tensor-valued function

$$\begin{aligned}
\bar{\mathbf{S}}_n[\mathbf{U}, \mathbf{U}, \ldots, \mathbf{U}] &\equiv \mathbf{S}_n[\mathbf{A}_n, \mathbf{A}_{n-1}, \ldots, \mathbf{A}_1] = \epsilon^n \mathbf{S}_n[\mathbf{a}_n, \mathbf{a}_{n-1}, \ldots, \mathbf{a}_1]\\
&\equiv \epsilon^n \bar{\mathbf{S}}_n[\underbrace{\mathbf{u}, \mathbf{u}, \ldots, \mathbf{u}}_{n \text{ times}}].
\end{aligned}$$

The stress tensors $\mathbf{S}_{(N)}$ for the fluids of grade N are determined when the Rivlin–Ericksen constants are known. The problem of viscometry for fluids of grade N is to find the value of the constants.

To summarize: the general problem of viscometry is to find the form of the stress response $\mathscr{F}$. This nearly intractable problem may be simplified by considering restricted problems of viscometry. We are interested in the restricted problem of viscometry associated with slow motions. We want to find the constants for the tensors $\mathbf{S}_{(N)}$.

3. Mechanical-response viscometers and free-surface viscometers

We are advocating the use of free-surface viscometers for the viscometry of the fluids of grade N. To understand free-surface viscometry better, it is useful to make comparisons with mechanical-response viscometry.

All of the viscometers based on viscometric flow theory are mechanical-response viscometers. The Couette viscometer is one example of a viscometric

† A complete discussion of all matters relating to (2.2) is given by Truesdell & Noll (1965, p. 494) and Truesdell (1974, p. 132).

mechanical-response viscometer.† The Couette viscometer gives values of the torque and, say, the normal thrust on the cylinder walls for given values of the angular velocity. Comparison of the experimental values with theoretical expressions based on viscometric flow theory can, in principle, yield the values of the three viscometric functions.

We have noted that viscometry based on the theory of viscometric flows has only a limited potential; given the three viscometric functions the response of the fluid is determined in all other viscometric flows, but not in more general flows.‡ In particular, complete knowledge of the viscometric functions will not determine the response of the fluid in most slow motions. Some, but not all, of the Rivlin–Ericksen constants, needed to determine the response of the fluid in slow flow, are defined by derivatives of the viscometric functions evaluated when the shear rate $\kappa = 0$. In principle, one could obtain some Rivlin–Ericksen constants by finding the values of the derivatives at $\kappa = 0$; in practice, this is difficult, because mechanical-response viscometers are inaccurate at low rates of shearing. It is unlikely that higher derivatives of the viscometric functions at $\kappa = 0$ could be computed by extrapolating experimental results for $\kappa = 0$.

Mechanical-response viscometers need not be restricted to viscometric flows. Such viscometers can be constructed to model any solution of the flow equations; in particular, the mechanical flow response of any slow flow that may be constructed as a perturbation from a state of rest may be used as a basis for a mechanical-response viscometer. Perturbation solutions pivoted around the rest state are naturally expressed in terms of the parameters of the Rivlin–Ericksen fluids. Mechanical-response viscometers may eventually be important for the viscometry of the fluids of grade N. The principal practical difficulty of mechanical-response viscometry for the fluids of grade N is that it is hard to get accurate results at low rates of shearing. This difficulty is particularly noxious, because the Rivlin–Ericksen constants are defined relative to the limit ($\kappa \to 0$) of zero shear. This practical problem of mechanical-response viscometry is, to a degree, avoided in free-surface viscometers.

A free-surface viscometer uses the shape of the free surface as a barometer for measuring the distribution of stresses at the surface. The free surface is very sensitive to changes in the forces at the surface and these types of viscometers have a demonstrated capacity to operate at low rates of shearing (Tanner 1970; Joseph *et al.* 1973).

The notion of a free-surface viscometer seems to have been first suggested by Wineman (see Pipkin & Tanner 1973). Wineman & Pipkin (1966) gave a perturbation theory for the problem of slow flow through a channel with vertical side walls containing fluid with a free surface on top. The bottom of the trough is tilted at an angle α from the horizontal. The free surface will bulge out, because

† A Couette viscometer is a mechanical device which models Couette flow – the flow induced by shearing the fluid between two infinitely long concentric cylinders rotating at different speeds. The flow in a Couette viscometer is a viscometric flow only if end effects in the apparatus are neglected.

‡ Despite efforts for over a decade, mechanical-response viscometry for viscometric flow has not led to a reliable determination of all three viscometric functions for a single non-Newtonian fluid (see Pritchard 1971; Pipkin & Tanner 1973).

it is pushed out by normal stresses associated with the shearing flow in the trough. The analysis is carried up to terms of order two in sin α. Surface tension is neglected. Tanner's (1970) experiments show good agreement between the height of the bulge and the angle.

A second kind of free-surface viscometer is associated with the Weissenberg effect. This effect describes the fact that, whereas the free surface near a rod rotating in a Newtonian fluid will fall, the free surface on, say, polymer solutions or whipping creams will rise. Joseph & Fosdick (1973) have given a perturbation theory of rod climbing, in which the climb depends on the Rivlin–Ericksen constants. By measuring the climb, Joseph *et al.* (1973) were able to determine the value of the combination of Rivlin–Ericksen constants (the climbing constant $\hat{\beta}$) that appears at lowest order in the perturbation expansion. Our present effort is one further step in the direction of establishing the rod-climbing theory and experiment as a 'rotating-rod viscometer'.

4. Mathematical formulation and the perturbation series

An infinitely long rod of radius a rotates with a steady angular velocity Ω in a vat of liquid under a free surface $z = h(r; \Omega)$. It is assumed that the air above the free surface cannot exert tangential tractions, and that the difference between the normal stress on the liquid side and the air pressure on the air side of the free surface is balanced by surface tension. The governing equations, written in cylindrical co-ordinates (r, θ, z) for axially symmetric velocity components $[u(r,z), v(r,z), w(r,z)]$ and without prior specification of the extra stress, are as follows: in $\mathscr{V}_\Omega$

$$\mathbf{u} = \mathbf{e}_\theta v + \mathbf{v}, \quad \mathbf{v} = \mathbf{e}_r u + \mathbf{e}_z w, \quad \frac{\partial ru}{\partial r} + \frac{\partial rw}{\partial z} = \nabla_2 . r\mathbf{v} = 0, \tag{4.1a}$$

$$\partial_r S_{rr} + \partial_z S_{rz} + \frac{1}{r}(S_{rr} - S_{\theta\theta}) - \partial_r \Phi = \rho \left[\mathbf{v} . \nabla_2 u - \frac{v^2}{r} \right], \tag{4.1b}$$

$$\frac{1}{r^2} \partial_r (r^2 S_{r\theta}) + \partial_z S_{z\theta} = \rho \left[\mathbf{v} . \nabla_2 v + \frac{uv}{r} \right] \tag{4.1c}$$

and

$$\partial_r S_{rz} + \partial_z S_{zz} + \frac{1}{r} S_{rz} - \partial_z \Phi = \rho \mathbf{v} . \nabla_2 w. \tag{4.1d}$$

$\Phi = p + \rho g z$ is the head; and

$$\nabla_2 = \mathbf{e}_r \partial_r + \mathbf{e}_z \partial_z.$$

At $r = a$,

$$\mathbf{u} = a\Omega \mathbf{e}_\theta. \tag{4.1e}$$

On the free surface $z = h(r; \Omega)$, we must satisfy the following conditions. The normal component of velocity must vanish:

$$w - h'u = 0 \quad (h' = dh/dr). \tag{4.1f}$$

The azimuthal and radial components of the shear stress must vanish:

$$S_{z\theta} - h' S_{r\theta} = 0 \tag{4.1g}$$

and

$$h'(S_{zz} - S_{rr}) + (1 - h'^2) S_{rz} = 0. \tag{4.1h}$$

The jump in the normal stress is balanced by the surface-tension force with surface tension T:

$$p_a - \Phi + S_{zz} - h' S_{rz} = (T/r)[rh'/(1+h'^2)^{\frac{1}{2}}]' - \rho g h. \tag{4.1i}$$

p_a is the air pressure. A contact angle $\hat{\phi}_a$ is prescribed at $r = a$:

$$h'(a;\Omega) = \cot\hat{\phi}_a. \tag{4.1j}$$

To complete the specification of the problem, we must properly pose conditions to be satisfied by solutions as $r \to \infty$ and $|z| \to \infty$. We shall require that all functions appearing in (4.1*a–e*) become independent of z as $-z \to \infty$. Far below the free surface, the flow is viscometric (we call it viscometric Couette flow) and it satisfies (5.1*a–e*) and (5.2*a–c*). As $r \to \infty$, the solution must approach the hydrostatic solution under a flat free surface

$$h(r;\Omega) \to 0, \quad \mathbf{u}(r,z;\Omega) \to 0, \quad \Phi \to 0 \quad \text{as} \quad r \to \infty. \tag{4.1k}$$

A closer specification of the asymptotic behaviour of solutions can be deduced by linearizing the problem around the asymptotic limit specified in (4.1*k*). This linearization is governed by the problem (5.11).

For very large values of $-z$, we shall require that the solution be fully developed, with a hydrostatic variation of pressure and a purely azimuthal velocity field depending only on r. This flow is defined more carefully in §5 when we consider the depth-averaged equations.

Free-surface problems like the one just described can be treated by a perturbation method in which the domain $\mathscr{V}_\Omega$ occupied by liquid and the flow both change with Ω. As in Joseph & Fosdick (1973), we first define a reference configuration as the domain $\mathscr{V}_0$ occupied by the fluid when $\Omega = 0$. We then define a mapping $\mathscr{V}_0 \leftrightarrow \mathscr{V}_\Omega$,

$$r = r_0, \quad z = \phi(r_0, z_0; \Omega), \quad -\infty < z \leqslant h(r;\Omega), \tag{4.2a}$$

which is even in Ω, and analytic in Ω, with

$$\phi(r_0, z_0; 0) = z_0, \quad -\infty < z_0 \leqslant h_0(r), \tag{4.2b}$$

which carries boundary points into boundary points:

$$\phi(r_0, h_0; \Omega) = h(r;\Omega). \tag{4.2c}$$

We expand the solution as a power series in the reference domain $\mathscr{V}_0$,

$$\begin{bmatrix} \mathbf{u}(r,z;\Omega] \\ h(r;\Omega) \end{bmatrix} = \sum_{n=0} \begin{bmatrix} \mathbf{u}^{[n]}(r_0,z_0) \\ h^{[n]}(r_0) \end{bmatrix} \Omega^n. \tag{4.3}$$

The square bracket superscripts denote a substantial derivative following the mapping (4.2*a*)

$$\mathbf{u}^{[n]}(r_0,z_0) = \frac{1}{n!}\frac{d^n\mathbf{u}}{d\Omega^n}\bigg|_{\Omega=0}. \tag{4.4}$$

These derivatives take account of the fact that the co-ordinate z depends on Ω. We also make heavy use of partial derivatives holding z fixed:

$$\mathbf{u}^{\langle n\rangle}(r_0,z_0) = \frac{1}{n!}\frac{\partial^n\mathbf{u}}{\partial\Omega^n}\bigg|_{\Omega=0}. \tag{4.5}$$

Since $h(r;\Omega)$ does not depend on z, $h^{\langle n\rangle}{}' = h^{[n]}$. The substantial derivatives and partial derivatives are connected by the chain rule

$$\mathbf{u}^{[1]} = \mathbf{u}^{\langle 1\rangle} + \phi^{\langle 1\rangle}\,\partial_z \mathbf{u}^{\langle 0\rangle},$$

$$\mathbf{u}^{[2]} = \mathbf{u}^{\langle 2\rangle} + \phi^{\langle 1\rangle}\,\partial_z \mathbf{u}^{\langle 1\rangle} + \tfrac{1}{2}(\phi^{\langle 1\rangle'})^2\,\partial_{zz}^2 \mathbf{u}^{\langle 0\rangle} + \phi^{\langle 2\rangle}\,\partial_z \mathbf{u}^{\langle 0\rangle},$$

etc.

The next task is to form the boundary-value problems for the substantial derivatives. One simplification is that (4.1 *a–e*) are identities in z, and they continue to hold when differentiated partially with respect to Ω. We may therefore write the perturbation field equations at nth order as

$$\nabla . \mathbf{u}^{\langle n\rangle} = 0, \tag{4.6a}$$

$$\rho(\mathbf{u}.\nabla\mathbf{u})^{\langle n\rangle} = -\nabla\Phi^{\langle n\rangle} + \mu\nabla^2\mathbf{u}^{\langle n\rangle} + \sum_{\substack{l+q=1+n\\ l\neq n}} \nabla . \mathbf{S}_q^{\langle l\rangle} \tag{4.6b}$$

in $\mathscr{V}_0$, and

$$\mathbf{u}^{\langle 1\rangle} = \mathbf{e}_\theta a, \quad \mathbf{u}^{\langle n\rangle} = 0 \quad (n \neq 1) \tag{4.6c}$$

at $r = a$. The tensors $\mathbf{S}_q^{\langle l\rangle}$ are defined in the following way. We first expand $\mathbf{u}(r,z;\Omega)$ to find

$$\left.\begin{aligned} \overline{\mathbf{S}}_n[\underbrace{\mathbf{u},\mathbf{u},\ldots,\mathbf{u}}_{n\text{ times}}] &= \sum_{l=1} \Omega^{l-1}\mathbf{S}_n^{\langle l\rangle},\\ \mathbf{S}_n^{\langle l\rangle} &= \Sigma_l \overline{\mathbf{S}}_n[\mathbf{u}^{\langle r_1\rangle}, \mathbf{u}^{\langle r_2\rangle}, \ldots, \mathbf{u}^{\langle r_n\rangle}]. \end{aligned}\right\} \tag{4.6d}$$

Σ_l is a summation over all integers $r_i \geqslant 1$ such that

$$l = \sum_{i=1}^{n} (r_i - n) + 1.$$

It follows that

$$\mathbf{S} = \sum_{n=1} \Omega^n \sum_{q+l=1+n} \mathbf{S}_q^{\langle l\rangle} \tag{4.6e}$$

on steady histories that are analytic in Ω.

To complete the specification of the perturbation problems, we must perturb the boundary conditions. The conditions are of the form $F(r,z;\Omega) = 0$ with $z = h(r;\Omega)$. Unlike the field equations, the boundary equations are not identities in z and, in general, $F^{\langle n\rangle} \neq 0$. Since $F(r, h(r;\Omega);\Omega) = 0$ identically in Ω, it follows that

$$0 = F^{[n]} = \left(\frac{\partial}{\partial\Omega} + h^{\langle 1\rangle}\frac{\partial}{\partial z}\right)^n F\Big|_{\Omega=0} \tag{4.6f}$$

for each of the boundary equations (4.1 *f–i*). It should be noted that the interior values of the mapping function ϕ do not enter into the perturbation problems generated by (4.6); only the boundary values $h^{\langle n\rangle}$ of the mapping are required, and these are determined sequentially as a part of the solution. Given $h(r;\Omega)$, we may define ϕ by the *shifting transformation*

$$r_0 = r, \quad z = \phi = z_0 + [h(r;\Omega) - h(r;0)]. \tag{4.7}$$

The problems (4.6) determine the rise coefficients $h^{\langle n\rangle}(r_0)$ and the velocity coefficients $\mathbf{u}^{\langle n\rangle}(r_0, z_0)$ as partial derivatives of the solution evaluated in the reference domain $\mathscr{V}_0$. Given the mapping function (4.7), we may obtain the

substantial derivatives $\mathbf{u}^{[n]}(r_0, z_0)$ once the velocity coefficients $\mathbf{u}^{\langle n\rangle}$ are known; e.g.

$$\mathbf{u}^{[1]} = \mathbf{u}^{\langle 1\rangle} + h^{\langle 1\rangle}\,\partial_z u^{\langle 0\rangle} \quad \text{for} \quad -\infty < z_0 \leqslant 0,$$

etc. Given the substantial derivatives in $\mathscr{V}_0$ we evaluate the solution in the deformed domain $\mathscr{V}_\Omega$ by inverting the shifting transformation (4.7):

$$\mathbf{u}(r, z; \Omega) = \sum_{n=0} \mathbf{u}^{[n]}(r_0, z_0)\,\Omega^n = \sum_{n=0} \mathbf{u}^{[n]}(r, z - h(r; \Omega))\,\Omega^n. \tag{4.8}$$

In this way it is possible to construct the perturbation solution on the domain $\mathscr{V}_\Omega$ of physical interest, while computing in the reference domain $\mathscr{V}_0$ chosen for mathematical convenience.†

In the rod-climbing problem, the most convenient of the reference domains is the one for which $h(r; 0) \equiv 0$. It is possible to use this convenient flat reference domain only if $h \equiv 0$ is a solution of the problem (4.1) when $\Omega = 0$. This solution is in fact unique, if the angle between the rod and the fluid is 90° (neutral wetting, $\hat{\phi}_a = \frac{1}{2}\pi$). Joseph *et al.* (1973) assumed neutral wetting, but neutral wetting did not hold in the experiments. They added a static contribution $h_s(r)$ to the h computed with $h'(a) = 0$; the static contribution was computed from the nonlinear surface-tension equation, using the values of the contact angle observed in the experiments. They gave some theoretical arguments and some experimental evidence to support this adding in of the static contribution. We shall examine this question in a more definitive way in this paper; by coating the rods we were able to get $h'(a) = 0$ in the experiments.

Adopting $h'(a) = 0$, we find, as in Joseph & Fosdick (1973), that

$$\mathbf{u}^{\langle 0\rangle} = \mathbf{S}^{\langle 0\rangle} = h^{\langle 0\rangle} \equiv h(r; 0) = 0 \quad \text{and} \quad \phi^{\langle 0\rangle} = 0.$$

The reference domain is now

$$\mathscr{V}_0 = [r_0, z_0 \,|\, a \leqslant r_0 < \infty,\ -\infty < z_0 \leqslant 0].$$

As a notational convenience, we shall denote the variables (r_0, z_0) as (r, z) wherever the context makes the intent clear. At first order, we find that

$$\left.\begin{aligned} -\nabla\Phi^{\langle 1\rangle} + \mu\nabla^2\mathbf{u}^{\langle 1\rangle} = 0, \quad \nabla\cdot\mathbf{u}^{\langle 1\rangle} = 0 \quad &\text{in} \quad \mathscr{V}_0, \\ \mathbf{u}^{\langle 1\rangle} = a\mathbf{e}_\theta \quad &\text{at} \quad r = a, \\ w^{\langle 1\rangle} = S^{\langle 1\rangle}_{z\theta} = S^{\langle 1\rangle}_{zr} = 0 \quad &\text{on} \quad z = 0, \end{aligned}\right\} \tag{4.9}$$

† The relation of Stokes' Eulerian theory of domain perturbations to the Lagrangian theory of Joseph, just described, is discussed in Joseph (1973) and in Joseph & Sturges (1975). To our knowledge, Stokes' theory does not deal with the problem of expressing the solution in the perturbed domain. The logical difficulties with Stokes' theory can be explained by a continuation argument resting on the identity (Joseph 1973, (6.2))

$$\sum_{n=0} \mathbf{u}^{[n]}(r_0, z_0) = \sum_{n=0} \mathbf{u}^{\langle n\rangle}(r, z(z_0; \Omega))\,\Omega^n.$$

The $\mathbf{u}^{\langle n\rangle}$ are functions determined by the perturbation problem in $\mathscr{V}_0$ extended, by declaration, onto $\mathscr{V}_\Omega\,(-\infty < z \leqslant h(r; \Omega))$. Of course, $\mathbf{u}^{\langle n\rangle}(r, h) \neq \mathbf{u}^{\langle n\rangle}(r, 0)$ and the extended functions do not agree with the restricted functions on the boundary. Equation (4.8) is a better way to express the solution in $\mathscr{V}_\Omega$, because each term of (4.8) satisfies a nice boundary condition and no arguments about analytic continuations are required.

with decay conditions for larger values of $-z$ and r. We find that

$$\mathbf{u}^{\langle 1\rangle} = \mathbf{e}_\theta a^2/r, \quad \Phi^{\langle 1\rangle} = 0. \tag{4.10}$$

The free-surface equation is

$$(rh^{\langle 1\rangle\prime})' - \rho g r h^{\langle 1\rangle} = 0, \quad h^{\langle 1\rangle\prime}(a) = 0.$$

Hence $h^{\langle 1\rangle} = 0$. At second order,

$$\left.\begin{aligned} \rho\mathbf{u}^{\langle 1\rangle}.\nabla\mathbf{u}^{\langle 1\rangle} &= -\nabla\Phi^{\langle 2\rangle} + \mu\nabla^2\mathbf{u}^{\langle 2\rangle} + \nabla.\mathbf{S}_2^{\langle 1\rangle} \quad \text{in} \quad \mathscr{V}_0, \\ \mathbf{u}^{\langle 2\rangle} &= 0 \quad \text{on} \quad r = a, \end{aligned}\right\} \tag{4.11}$$

where

$$\left.\begin{aligned} \mathbf{u}^{\langle 1\rangle}.\nabla\mathbf{u}^{\langle 1\rangle} &= -\mathbf{u}_\theta^{\langle 1\rangle 2}\frac{\mathbf{e}_r}{r} = -\frac{a^4\mathbf{e}_r}{r^3}, \\ \nabla\mathbf{u}^{\langle 1\rangle} &= \mathbf{e}_r\mathbf{e}_\theta\frac{du_\theta^{\langle 1\rangle}}{dr} - \frac{\mathbf{e}_\theta\mathbf{e}_r u_\theta^{\langle 1\rangle}}{r}, \\ \mathbf{A}_1[\mathbf{u}^{\langle 1\rangle}] &= (\mathbf{e}_r\mathbf{e}_\theta + \mathbf{e}_\theta\mathbf{e}_r)\left(\frac{du_\theta^{\langle 1\rangle}}{dr} - \frac{u_\theta^{\langle 1\rangle}}{r}\right), \\ \mathbf{A}_2[\mathbf{u}^{\langle 1\rangle}] &= \mathbf{u}^{\langle 1\rangle}.\nabla\mathbf{A}_1 + \nabla\mathbf{u}^{\langle 1\rangle}.\mathbf{A}_1 + (\nabla\mathbf{u}^{\langle 1\rangle}.\mathbf{A}_1)^T = 2\left(\frac{du_\theta^{\langle 1\rangle}}{dr} - \frac{u_\theta^{\langle 1\rangle}}{r}\right)\mathbf{e}_r\mathbf{e}_r, \end{aligned}\right\} \tag{4.12}$$

$$\begin{aligned} \mathbf{S}_2^{\langle 1\rangle} &= \alpha_1\mathbf{A}_2[\mathbf{u}^{\langle 1\rangle}] + \alpha_2\mathbf{A}_1^2[\mathbf{u}^{\langle 1\rangle}] \\ &= [(2\alpha_1+\alpha_2)\,\mathbf{e}_r\mathbf{e}_r + \alpha_2\mathbf{e}_\theta\mathbf{e}_\theta]\left(\frac{du_\theta^{\langle 1\rangle}}{dr} - \frac{u_\theta^{\langle 1\rangle}}{r}\right)^2 \\ &= \frac{4a^4}{r^4}[(2\alpha_1+\alpha_2)\,\mathbf{e}_r\mathbf{e}_r + \alpha_2\mathbf{e}_\theta\mathbf{e}_\theta], \end{aligned} \tag{4.13}$$

and

$$\nabla.\mathbf{S}_2^{\langle 1\rangle} = -\mathbf{e}_r\frac{8a^4}{r^5}(3\alpha_1+2\alpha_2). \tag{4.14}$$

To obtain the boundary conditions at $z = 0$, we note that, since $h^{\langle 1\rangle} = 0$ and $\partial_z f^{\langle 0\rangle} = 0$, where f stands for any of the variables of the rest state,

$$(.)^{[2]} = (.)^{\langle 2\rangle} + h^{\langle 2\rangle}\partial_z(.)^{\langle 0\rangle} = (.)^{\langle 2\rangle}.$$

It follows that

$$w^{\langle 2\rangle} = S_{z\theta}^{\langle 2\rangle} = S_{rz}^{\langle 2\rangle} = \Phi^{\langle 2\rangle} - S_{zz}^{\langle 2\rangle} + (T/r)\,(rh^{\langle 2\rangle\prime})' - \rho g h^{\langle 2\rangle} = 0,$$

where

$$\mathbf{S}^{\langle 2\rangle} = \mathbf{S}_2^{\langle 1\rangle} + \mathbf{S}_1^{\langle 2\rangle} = \mathbf{S}_2^{\langle 1\rangle} + \mu\mathbf{A}_1[\mathbf{u}^{\langle 2\rangle}],$$

and $\mathbf{S}_2^{\langle 1\rangle}$ is given by (4.13).

We note next that

$$\nabla.\mathbf{S}_2^{\langle 1\rangle} - \rho\mathbf{u}^{\langle 1\rangle}.\nabla\mathbf{u}^{\langle 1\rangle} = \mathbf{e}_r\frac{d}{dr}\left[\frac{2a^4}{r^4}(3\alpha_1+2\alpha_2) - \frac{\rho a^4}{2r^2}\right]$$

is a gradient, and may be equilibrated by a pressure (without motion $u^{\langle 2\rangle} = v^{\langle 2\rangle} = w^{\langle 2\rangle} = 0$)

$$\Phi^{\langle 2\rangle} = \frac{2a^4}{r^4}\hat{\beta} - \frac{\rho a^4}{2r^2}. \tag{4.15}$$

$\hat{\beta} = 3\alpha_1 + 2\alpha_2$ is the climbing constant. The coefficient $h^{\langle 2\rangle}(r)$, which gives the first deviation of the free surface from flatness, is determined from the problem

$$\frac{T}{r}(rh^{\langle 2\rangle\prime})' - \rho g h^{\langle 2\rangle} = -\frac{2a^4}{r^4}\hat{\beta} + \frac{\rho a^4}{2r^2}, \tag{4.16a}$$

$$h^{\langle 2\rangle\prime}(a) = 0, \quad h^{\langle 2\rangle}(r) \to 0 \quad \text{as} \quad r \to \infty. \tag{4.16b}$$

The properties of $h^{\langle 2\rangle}$ were thoroughly discussed in Joseph *et al.* (1973). For completeness, we shall summarize that discussion here.

The fluid will climb the rod whenever Ω is small and wherever $h^{\langle 2\rangle}(r) > 0$. To see this, it is convenient to set $T = 0$. Then the free surface will rise if and only if $\hat{\beta} > 0$ and

$$r^2 < 4\hat{\beta}/\rho.\dagger \tag{4.17}$$

Otherwise, inertia dominates, and the free surface sinks. Representative values for $\hat{\beta}$ near room temperatures in our experiments are $\hat{\beta} \approx 1$ (STP) and $\hat{\beta} \approx 0{\cdot}8$ and $1{\cdot}4$ (polyacrylamide). It is easy to verify that the ratio

$$|T(rh^{\langle 2\rangle\prime})'/\rho g r h^{\langle 2\rangle}| \to 16T/\rho g r^2$$

as $r \to 0$ when $h^{\langle 2\rangle}$ is given (4.16*a*) with $T = 0$. This ratio shows that when r is small surface tension should not be neglected. To determine the way in which the parameters $a, \hat{\beta}, \rho, g, T$ affect $h^{\langle 2\rangle}$, Joseph *et al.* (1973) derived an accurate approximation to the problem (4.16*a*, *b*). In the approximation, we write (4.16*a*) as

$$Tr(rh^{\langle 2\rangle\prime})' - \rho g a^2 h^{\langle 2\rangle} = -a^2\Phi^{\langle 2\rangle} + (r - a^2/r)\,T(rh^{\langle 2\rangle\prime})'. \tag{4.18}$$

The last term of (4.18) is zero when $r = a$. We set this term to zero, and solve the remaining problem; then we restore the neglected term through successive approximations. The first approximation is very accurate, especially near the rod $r = a$ (see Joseph *et al.* 1973):

$$h^{\langle 2\rangle} \sim \frac{a}{2T\sqrt{S}}\left[\frac{4\hat{\beta}}{4+\lambda} - \frac{\rho a^2}{2+\lambda}\right]. \tag{4.19}$$

$\lambda^2 = a^2 S$ and $S = \rho g/T$. This expression shows that, when a is small, $h^{\langle 2\rangle}$ is proportional to a and $\hat{\beta}$, and is inversely proportional to $T^{\frac{1}{2}}$.

† The first theoretical analyses of rod climbing are due to Serrin (1959) and Giesekus (1961). Serrin studied the problem for a Reiner–Rivlin fluid with constant coefficients (for this mathematical fluid, $\hat{\beta} = 2\alpha_2$), on the assumption that the free surface was nearly flat and that the z dependence of the solution and the secondary motions could be neglected. Surface tension was neglected. He interpreted a negative slope at $r = a$ as a tendency to climb and a negative slope at $r = b$ as a tendency to fall. This criterion is not well suited to problems involving surface tension. Serrin found that, in the case $b \gg a$, the fluid has a tendency to climb (in his sense) if $a < 2(2\alpha_2/\rho)^{\frac{1}{2}}$. This result is consistent with and implied by (4.17), which Joseph *et al.* (1973) deduced by setting $T = 0$. Giesekus (1961), independently, studied rod climbing of a second-order fluid by the same approximate method used by Serrin. But Giesekus neglected inertia and did not deduce a critical radius. Fosdick & Serrin (1974, private communication) have shown that the critical radius $2(\hat{\beta}/\rho)^{\frac{1}{2}}$ continues to have significance when rod climbing is assumed to be governed by an equation which is like (4.16*a*), except that the nonlinear surface-tension term is retained and arbitrarily prescribed contact angles are allowed.

Returning now to general remarks about the perturbation solution, we note that an unexpected feature of the solution is that no secondary motions are generated at second order. This makes it possible to find the first correction for the shape of the free surface, without solving the difficult fourth-order problem governing the motion. The condition that $h'(a) = 0$ is absolutely essential in this mathematical result; without it, the reference domain would not be flat and, as we shall explain, secondary motion would be generated by an unequilibrated shear stress on the free surface. Actual secondary motions induced in this way may be very weak.

We shall not pursue the perturbation analysis further; the analysis up to order four is given in Joseph & Fosdick (1973), and only a very small part of the higher-order theory is needed to achieve the aims of this paper. It is necessary, however, to display the ordering of the formal solution in powers of Ω, and it is helpful to explain this ordering in physical terms.

The head ($\Phi = p + \rho g z$), the pressure p, the free surface, and secondary motion should not change when the rod is rotated the other way; therefore, the power series solution will be in even powers of Ω. The azimuthal component of velocity, and the associated stress should change sign with Ω. It follows that

$$h(r;\Omega) = h^{\langle 2\rangle}(r)\,\Omega^2 + O(\Omega^4),$$
$$\Phi(r,z;\Omega) = p + \rho g z = \Phi^{\langle 2\rangle}\Omega^2 + O(\Omega^4),$$
$$\mathbf{u}(r,z;\Omega) = \mathbf{e}_\theta[u_\theta^{\langle 1\rangle}\,\Omega + O(\Omega^3)] + \nabla \times [\mathbf{e}_\theta\{\psi^{\langle 4\rangle}(r,z)\,\Omega^4 + O(\Omega^6)\}].$$

The velocity field $\mathbf{u}$ has been split into an azimuthal component and a secondary motion, which is given by derivatives of a stream function $\psi(r,z;\Omega)$.

There is a neat sorting of the different characteristic physical effects into an association with the different powers of Ω in the series solution. When there is no rotation, the free surface is flat and the pressure is hydrostatic. At first order in Ω, there is a z-independent flow in circles with no change in the pressure or flat free surface. At order two, the pressure must equilibrate the central forces arising from centripetal accelerations and normal stress. The free surface acts as the barometer of the interior pressure distribution, rising where the interior pressure is greatest. The free surface can remain flat only if there is no motion. The departure from flatness of the free surface at order two requires that the azimuthal velocity, at order three, should come to depend on z. This is a con sequence of the fact that the azimuthal component of the shear stress

$$S_{n\theta} = S_{z\theta} - h' S_{r\theta},$$

which vanishes automatically for z-independent fields when the free surface is flat, can vanish when the free surface is not flat only when $S_{z\theta} = h' S_{r\theta}$ does not vanish. The z dependence of the azimuthal field at third order is generated without changing the pressure or the shape of the free surface. The z-dependent azimuthal field, generated at order three, is associated at order four with forces that also depend on z; such forces inevitably exert torques in an azimuthal plane, and they lead to secondary motions.

This ends our discussion of the perturbation theory. A more complete derivation of the theory including higher orders (through Ω^4), and some solutions can

be found in Joseph & Fosdick (1973). The evaluation of the higher-order theory at order Ω^4, where the secondary motions first appear, is important; our experiments show very little deviation from what might be expected of a fourth-order theory (see figure 17).

In the next section we shall reformulate the problem of rod climbing without perturbations.

5. The depth-averaged difference equations and the invariance of the torque

Difference equations may be formed by subtracting from the basic equations (4.1) the equations ((5.1) below) which govern the viscometric flow that prevails far below the free surface. Vertical averaging converts the partial differential equations into a formally much simpler set of ordinary, integral–differential equations. Much of the simplicity of form achieved in depth averaging arises from the way that conditions at the free boundary are put into the equations.

Consider the viscometric Couette flow, designated with a tilde overbar, to which solutions of (4.1) tend far below the free surface. The equations that govern this flow are

$$\left.\begin{aligned} \tilde{u} = \tilde{w} = \tilde{S}_{z\theta} = \tilde{S}_{zz} = 0, & \qquad (5.1a)\\ \tilde{S}'_{rr} + \frac{1}{r}(\tilde{S}_{rr} - \tilde{S}_{\theta\theta}) - \tilde{\Phi}' = -\frac{\rho\tilde{v}^2}{r}, & \qquad (5.1b)\\ (r^2\tilde{S}_{r\theta})' = 0, & \qquad (5.1c) \end{aligned}\right\} \quad a \leqslant r \leqslant \infty,$$

$$\tilde{\mathbf{u}}(a) = \mathbf{e}_\theta a\Omega, \quad \tilde{v}(r) \to 0 \quad \text{as} \quad r \to \infty. \qquad (5.1d, e)$$

The stresses in a viscometric flow are

$$\begin{bmatrix} \tilde{S}_{rr} & \tilde{S}_{r\theta} & 0 \\ \tilde{S}_{r\theta} & \tilde{S}_{\theta\theta} & 0 \\ 0 & 0 & 0 \end{bmatrix} = \begin{bmatrix} \sigma_1(\kappa) & \kappa\mu(\kappa) & 0 \\ \kappa\mu(\kappa) & \sigma_2(\kappa) & 0 \\ 0 & 0 & 0 \end{bmatrix}.$$

$\sigma_1(\kappa)$, $\sigma_2(\kappa)$ and $\kappa\mu(\kappa)$ are the three scalar functions of the rate of shearing

$$\kappa = 2D_{r\theta} = r\omega'(r);$$

$\omega = v/r$ is the angular velocity function. Equations (5.1) may be integrated:

$$r^2\tilde{S}_{r\theta}(r) = a^2\tilde{S}_{r\theta}(a), \qquad (5.2a)$$

$$\tilde{\Phi}(r) = C_1 + f(r) = p_a + f(r), \qquad (5.2b)$$

where

$$f(r) = \tilde{S}_{rr}(r\omega') + \int^r \frac{1}{r}(\tilde{S}_{rr} - \tilde{S}_{\theta\theta})\,dr + \rho\int^r r\tilde{\omega}^2 dr \qquad (5.2c)$$

has no constant part. The constant $C_1 = p_a$ in (5.2b) is selected so that $\Phi(r, z)$ and $\tilde{\Phi}(r)$ will have a common limiting value on the free surface $z = 0$ as $r \to \infty$. The velocity field may be determined by integrating (5.2a) subject to the no-slip condition.

The difference between solutions (4.1) and (5.1) is designated with a double bracket:

$$[[\,.\,]] = (\,.\,) - \tilde{(\,.\,)}.$$

Subtracting (5.1) from (4.1), we find the following. Under $z = h(r;\Omega)$,

$$\partial_r(r[[S_{rr}]]) - [[S_{\theta\theta}]] - r\,\partial_r[[\Phi]] + r\,\partial_z S_{rz} = \rho(\nabla_2 . ru\mathbf{v} - [[v^2]]), \tag{5.3a}$$

$$\frac{1}{r}\,\partial_r(r^2[[S_{r\theta}]]) + r\,\partial_z S_{z\theta} = \rho(\nabla_2 . rv\mathbf{v} + uv), \tag{5.3b}$$

$$\partial_r(rS_{rz}) + r\partial_z(S_{zz} - [[\Phi]]) = \rho\nabla_2 . rw\mathbf{v}, \tag{5.3c}$$

where $\mathbf{v} = \mathbf{e}_r u + \mathbf{e}_z w$ and $\mathbf{v}$ satisfies (4.1*a*). On $z = h$, we have (4.1*f*) and

$$S_{z\theta} - h'\tilde{S}_{r\theta} - h'[[S_{r\theta}]] = 0, \tag{5.3d}$$

$$h'S_{zz} - h'[[S_{rr}]] - h'\tilde{S}_{rr} + (1-h'^2)\,S_{rz} = 0, \tag{5.3e}$$

and

$$S_{zz} - h'S_{rz} - [[\Phi]] - f(r) = (T/r)\,[rh'/(1+h'^2)^{\frac{1}{2}}]' - \rho gh. \tag{5.3f}$$

The depth-averaged equations, (5.5) below, may be obtained from (5.3*a*–*c*) by integration over z at a fixed value of r:

$$\langle . \rangle = \int_{-\infty}^{h} . \, dz, \tag{5.4}$$

$$\langle r[[S_{rr}]]\rangle' - \langle [[S_{\theta\theta}]]\rangle - r\langle [[\Phi]]\rangle' - h'[T[rh'/(1+h'^2)^{\frac{1}{2}}]' - \rho grh + rf(r) - r\bar{S}_{rr}]$$
$$= \rho(r\langle u^2\rangle)' - \rho\langle [[v^2]]\rangle, \tag{5.5a}$$

$$(r^2\langle [[S_{r\theta}]] - \rho uv\rangle)' + r^2h'\tilde{S}_{r\theta} = 0, \tag{5.5b}$$

and

$$\langle rS_{rz} - \rho rwu\rangle' + T[rh'/(1+h'^2)^{\frac{1}{2}}]' - \rho grh + rf = 0. \tag{5.5c}$$

These equations will be derived later. They are, of course, equivalent to the original set (5.3*a*–*c*). This set is formally simpler than the equations (5.3*a*–*c*) from which they were derived. Equations (5.5) may be useful in global analysis of rod climbing using Galerkin or other approximate methods.

Equation (5.5*c*) could be regarded as the rod-climbing equation. When the secondary motion and surface tension are both neglected, the first two terms of (5.5*c*) vanish. The equation $\rho gh = f$ was first studied by Serrin (1959). More recently, Fosdick & Serrin (1974, private communication) studied (5.5*c*) neglecting secondary motion, and with $f = \Phi^{(2)}$.

It is possible to deduce from (5.5*b*) a surprising theorem about the invariance of torque in steady axisymmetric flow. We shall first give a rough, then a precise, statement of this theorem.

Consider the torque on two rods of the same diameter, rotating with angular velocity Ω in separate samples of the same simple fluid. One of the rods generates a steady axisymmetric flow under the free surface $z = h$. The other is infinitely long, and it generates a viscometric Couette flow of fluid filling all space. Suppose the rod under the free surface $z = h$ has a sufficiently long length l. *The torque on a length $l+h$ of rod in the flow under $z = h$ is the same as the torque on a length l of rod in viscometric Couette flow.* This is the rough statement. What we actually prove is that

$$T_Q(\Omega, \mathscr{V}_\Omega) - \tilde{T}_Q(\Omega, \mathscr{V}_0) = 0, \tag{5.6}$$

where

$$T_Q(\Omega, \mathscr{V}_\Omega) = 2\pi a \int_{-\infty}^{h(r)} S_{r\theta}(a, z; \Omega)\, dz$$

is the torque on an infinitely long rod rotating under the free surface $z = h$, and

$$\tilde{T}_Q(\Omega, \mathscr{V}_0) = 2\pi a \int_{-\infty}^{0} \tilde{S}_{r\theta}(a; \Omega)\, dz$$

is the torque on the bottom half of the infinitely long rod rotating in viscometric Couette flow. Both torques are infinite; but, if

$$|S_{r\theta}(a, z; \Omega) - \tilde{S}_{r\theta}(a; \Omega)| = o(z^{-1}) \tag{5.7}$$

as $z \to -\infty$, then the difference

$$T_Q(\Omega, \mathscr{V}_\Omega) - \tilde{T}_Q(\Omega, \mathscr{V}_0)$$

is finite. In fact, (5.7) is probably an overly conservative estimate of the decay of the flow under $z = h$ into viscometric form. The discrepancy between viscometric flow and the flow under $z = h$ stems from the free surface, and the action of secondary flows is probably confined to a region about the order of a rod diameter. More likely than (5.7) is the estimate

$$|S_{r\theta}(a, z; \Omega) - \tilde{S}_{r\theta}(a; \Omega)| = O(\exp kz), \tag{5.8}$$

where $k(a) > 0$ is $O(a)$. The estimates (5.7) or (5.8) imply that there is a value $l(\epsilon)$ such that

$$\int_{-\infty}^{-l(\epsilon)} |S_{r\theta}(a, z; \Omega) - \tilde{S}_{r\theta}(a; \Omega)|\, dz < \epsilon$$

for any $\epsilon > 0$. This is the rod length $l = l(\epsilon)$ in our rough statement.

To prove (5.6), we note that (5.2a) implies that

$$r^2 \tilde{S}_{r\theta}(r; \Omega) = a^2 \tilde{S}_{r\theta}(a; \Omega).$$

Then, replacing $r^2\tilde{S}_{r\theta}$ in the second term of (5.5b), we may integrate (5.5b) from a to r. We find that

$$a^2 \langle [[S_{r\theta}]] \rangle|_{r=a} - r^2 \langle [[S_{r\theta}]] - \rho uv \rangle + a^2 \tilde{S}_{r\theta}(a; \Omega)\, [h(a; \Omega) - h(r; \Omega)] = 0. \tag{5.9}$$

Since $h \to 0$ as $r \to \infty$, the second term of (5.9) is bounded. An even stronger result holds:

$$r^2 \langle [[S_{r\theta}]] - \rho uv \rangle \to 0. \tag{5.10}$$

To prove (5.10), we note that, where $r \to \infty$, (4.1k) holds and we may linearize the equations around the hydrostatic solution. Since $\mathbf{u} \to 0$ where r is large, we may assume that the linearization of the stress response is a Newtonian response. This linearization is used in what follows to show that $[[\partial v/\partial r]] = [[S_{r\theta}]]/\mu$ and uv are $o(1/r^2)$. Under linearization, (5.3b), (5.3d), (5.3f) and conditions specified for $-z \to \infty$ under (4.1k) may be written respectively as

$$\frac{1}{r}\partial_r\left(r^2\left[\left[\frac{\partial v}{\partial r}\right]\right]\right) + r\partial_z\left[\left[\frac{\partial v}{\partial z}\right]\right] = 0, \tag{5.11a}$$

$$\left[\left[\frac{\partial v}{\partial z}\right]\right] = \text{const.}\frac{h'}{r^2} \quad \text{on} \quad z = h \to 0, \tag{5.11b}$$

$$h = \frac{f(r)}{\rho g} = O\left(\frac{1}{r^2}\right), \tag{5.11c}$$

and, for all $r \geqslant a$,
$$\lim_{-z\to\infty} v(r,z) = \tilde{v}(r) = a^2\Omega/r. \tag{5.11d}$$

Equation (5.11*d*) may be expressed as
$$\lim_{-z\to\infty} [[v]] = 0.$$

Equations (5.11*a–c*) now imply that, on the free surface,
$$[[v]] = O(1/r^5), \quad \left[\left[\frac{\partial v}{\partial r}\right]\right] = \frac{[[S_{r\theta}]]}{\mu} = O\left(\frac{1}{r^6}\right).$$

It is now easy to see, by linearizing (4.1*b*), that $u = o(1/r)$ and $uv = o(1/r^2)$, proving (5.10).

Equations (5.9) and (5.10) imply that
$$\int_{-\infty}^{h(a;\Omega)} [S_{r\theta}(a,z;\Omega) - \tilde{S}_{r\theta}(a;\Omega)]\,dz + h(a;\Omega)\,\tilde{S}_{r\theta}(a;\Omega) = 0.$$

Moreover,
$$h(a;\Omega)\,\tilde{S}_{r\theta}(a;\Omega) = \int_{-\infty}^{h(a;\Omega)} \tilde{S}_{r\theta}(a;\Omega)\,dz - \int_{-\infty}^{0} \tilde{S}_{r\theta}(a;\Omega)\,dz.$$

Hence,
$$\int_{-\infty}^{h(a;\Omega)} S_{r\theta}(a,z;\Omega)\,dz = \int_{-\infty}^{0} \tilde{S}_{r\theta}(a;\Omega) \quad \text{or} \quad T_Q(\Omega,\mathscr{V}_\Omega) = \tilde{T}_Q(\Omega,\mathscr{V}_0),$$

proving (5.6).

The physical meaning of the torque theorem can best be expressed by comparing the torques over the region $-l(\epsilon) < z < h$, where the flow under the free surface is perceptibly different from viscometric Couette flow. Assuming (5.7) or (5.8), there is $l(\epsilon) > 0$ such that for any $\epsilon > 0$
$$\left|\frac{T_Q(\Omega,\mathscr{V}_\Omega)}{l(\epsilon)+h} - \frac{l(\epsilon)}{l(\epsilon)+h}\frac{\tilde{T}_Q(\Omega,\mathscr{V}_0)}{l(\epsilon)}\right| < \epsilon. \tag{5.12}$$

This expression implies that the torque per unit length $T_Q(\Omega,\mathscr{V}_\Omega)/(l+h)$ in a climbing flow (STP) is smaller, and in a sinking flow is larger, than the torque per unit length $\tilde{T}_Q(\Omega,\mathscr{V}_0)/l$ on the same rod rotating in a viscometric flow. For a Newtonian fluid,
$$\tilde{T}_Q(\Omega,\mathscr{V}_0)/l = -4\pi a\mu\Omega$$
is independent of l. The estimate (5.12) gives more information when the region ($l(\epsilon)$ for small ϵ), over which the flow is disturbed, is not too large.

It remains finally to derive the depth-averaged equations (5.5*a–c*). The derivation uses the following identities. If $g(r,z)$ is any smooth integrable function, then
$$\begin{aligned}\langle \partial_r g\rangle &= \int_{-\infty}^{h(r)} \partial_r g\,dz = \frac{d}{dr}\int_{-\infty}^{h} g\,dz - h'(r)\,g(r,h)\\ &= \langle g\rangle' - h'(r)\,g(r,h).\end{aligned} \tag{5.13}$$

If $\mathbf{v} = \mathbf{e}_r u + \mathbf{e}_z w$ is any smooth integrable field satisfying (4.1*f*), then
$$\begin{aligned}\langle \nabla_2 . r\mathbf{v} g\rangle &= \int_{-\infty}^{h} \left[\frac{\partial}{\partial r}(rug) + \frac{\partial}{\partial z}(rwg)\right] dz\\ &= \langle rug\rangle' + rg(w - h'u) = (r\langle ug\rangle)'.\end{aligned} \tag{5.14}$$

It follows from (5.14) that

$$\langle uv + \nabla_2 . rv\mathbf{v}\rangle = \langle uv\rangle + (r\langle uv\rangle)' = (1/r)\,(r^2\langle uv\rangle)'. \tag{5.15}$$

Applying (5.13) and (5.14) to (5.3a), we get

$$\langle r[[S_{rr}]]\rangle' - \langle[[S_{\theta\theta}]]\rangle - r\langle[[\Phi]]\rangle' - rh'[[S_{rr} - \Phi]]|_{z=h} + rS_{rz}|_{z=h} = \rho(r\langle u^2\rangle)' - \rho\langle[[v^2]]\rangle. \tag{5.16a}$$

Applying (5.13) and (5.15) to (5.3b), we get

$$\frac{1}{r}\langle r^2[[S_{r\theta}]]\rangle' - r[h'[[S_{r\theta}]] - S_{z\theta}]|_{z=h} = \frac{\rho}{r}(r^2\langle uv\rangle)'. \tag{5.16b}$$

Applying (5.13) and (5.14) to (5.3c), we get

$$\langle rS_{rz}\rangle' - r[h'S_{rz} - (S_{zz} - [[\Phi]])]|_{z=h} = \rho\langle rwu\rangle'. \tag{5.16c}$$

To obtain (5.5a), we combine (5.16a), (5.3e) and (5.3f). To obtain (5.5b), we combine (5.16b) and (5.3d). To obtain (5.5c), we combine (5.16c) and (5.3f). This completes the derivation of the depth-averaged equations (5.5a–c).

6. The method of slopes and the method of profile fitting

The perturbation theory of the rotating rod viscometer may possibly be used to determine the Rivlin–Ericksen parameters up to order four. We are now going to establish the utility of the theory up to order two; the higher-order theory will be discussed briefly in § 8.

We use the second-order theory to determine the values of the constant $\hat{\beta}$ from (6.1) below:

$$h(r;\Omega^2,\hat{\beta},\rho,T) = h^{\langle 2\rangle}(r;\hat{\beta},\rho,T)\,\Omega^2 + O(\Omega^4).\dagger \tag{6.1}$$

When h, T and ρ are given, we may compute $\hat{\beta}$ from (6.1). In figures 9, 12, 18 and 22, we have plotted typical examples of the height rise at $r = a$ against the square of the angular velocity $\omega^2 = \Omega^2/4\pi^2$. As was true of the Joseph *et al.* (1973) experiments, the rise is nearly linear in ω^2 for values of ω^2 less than about 10. This suggests that there might be good agreement between the second-order theory given by (6.1) and the experimental observations. Such agreement was attained in Joseph *et al.* (1973), even though in those experiments the condition $h'(a) = 0$ was not satisfied; neither was $h'(a)$ small. Joseph *et al.* (1973) attributed the rise associated with the non-zero wetting angle $h'|_{r=a} = -\epsilon$ to capillarity. We replaced (6.1) with

$$h(r;\Omega^2,\hat{\beta},\rho,T,\epsilon) = h_s(r;\rho,T,\epsilon) + h^{\langle 2\rangle}(r;\hat{\beta},\rho,T)\,\Omega^2 + O(\Omega^2\epsilon + \Omega^4). \tag{6.2}$$

† It is best to regard $h^{\langle 2\rangle}$ as the slope of the rise curve at the origin of the Ω^2, h plane. The existence of a substantial interval of ω^2 ($= \Omega^2/4\pi^2$) over which the rise is linear is an accident which requires that the remainder in (6.1) be small relative to $h^{\langle 2\rangle}\Omega^2$ (see Joseph *et al.* 1973, p. 385, footnote).

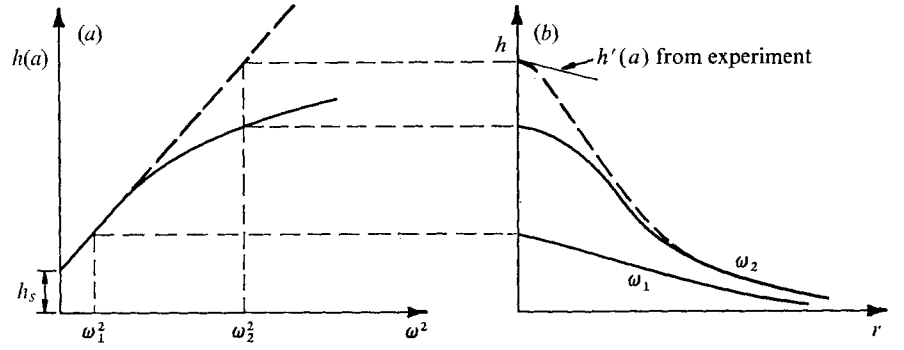

FIGURE 2. (*a*) Method of slopes. (*b*) Method of profile fitting. – – –, second-order theory; ——, experiment. Observed rise at $r = a$ never seems to lie above second-order theory. Static rise in height h_s computed using observed contact angles. When the fluid does not wet the rod, $h_s = 0$ and $h'(a) = 0$. In second-order theory $\hat{\beta}$ is computed from (6.5) by method of slopes. Theoretical profiles computed numerically from first two terms of (6.2) using observed values of $h'(a)$, and values of $\hat{\beta}$ taken from method of slopes.

h_s is the static rise, computed from

$$\frac{T}{r}\left[\frac{rh_s'}{(1+h_s'^2)^{\frac{1}{2}}}\right]' - \rho g h_s = 0, \quad h'|_{r=a} = -\epsilon, \cdot\ h_s \to 0 \quad \text{as} \quad r \to \infty. \tag{6.3}$$

The static rise vanishes when $\epsilon = 0$. The plausible procedure (6.2) for computing h seemed to work, but had an *ad hoc* character, since ϵ was not small and there was no *a priori* reason to neglect terms $O(\Omega^2\epsilon)$. In the new experiments reported here, we have been able to control ϵ, setting it to zero.

There are two methods we use to determine $\hat{\beta}$ from (6.2) and the measured values of $h = h_{\text{exp}}$: the method of slopes and the method of profile fitting. The two methods are demonstrated in figure 2. To use the method of slopes, we need only measure the height rise h_{exp} at $r = a$; from these measurements, we read off a slope and equate the theoretical and measured values

$$h^{\langle 2\rangle}(a; \hat{\beta}, \rho, T) = dh_{\text{exp}}/d\Omega^2. \tag{6.4}$$

This equation is then solved for $\hat{\beta}$. The method of slopes does not depend on the static climb h_s, but the only justification we have for assuming that $dh_{\text{exp}}/d\Omega^2$ is independent of ϵ is experimental.

In the method of profile fitting, we choose the value of $\hat{\beta}$ that gives the best fit over the entire profile. This method is judged successful if, at a given temperature, one and the same value of $\hat{\beta}$ is determined for a single fluid from tests with rods of different radius rotating at different values of Ω. The method of profile fitting requires that one compute the static rise h_s from the experimentally measured values of ϵ. The method of profile fitting is more accurate but more time-consuming than the method of slopes. In general, the determination of $\hat{\beta}$ is achieved most efficiently and accurately by simultaneous use of both methods.

In using these two methods, we have noticed that the experimentally measured rise curves never lie above the rise curve predicted from the second-order theory.

The observed curves must, by construction, coincide in value and slope with the theoretical curve when $\Omega = 0$.† The second-order curve is a straight line of slope

$$\left.\frac{dh}{d\Omega^2}\right|_{\Omega=0} = h^{(2)}|_{r=a} \approx \frac{a}{2TS^{\frac{1}{2}}}\left[\frac{4\hat{\beta}}{4+\lambda} - \frac{\rho a^2}{2+\lambda}\right], \tag{6.5}$$

where $\lambda^2 = a^2S$ and $S = \rho g/T$. The observed curve has a one-signed curvature; it bends down and away from the straight line. It follows that the theoretically computed profiles lie above (never below) the observed ones when r is near to a. The discrepancy between the computed and measured values of the rise at $r = a$ must tend to zero monotonically with Ω.

7. Experimental equipment

The essential part of the viscometer is a circular rod, which is free to rotate about a vertical axis in a large vat of fluid. The principal components of the viscometer, as shown in figure 3 (plate 2), include a drive motor, an accurately machined circular rod, and a large container of liquid. The viscometer is mounted on a heavy steel table to minimize external disturbances. During operation of the viscometer, the part of the apparatus shown in figure 3 is enclosed in a glass-fronted cabinet, within which the temperature can be maintained within $\pm 0{\cdot}25$ °C of any pre-selected value between about 25 and 50 °C. A recirculating forced-air heating system is used to accomplish this. The liquid temperature is monitored by means of a thermocouple located in the liquid, and the output is amplified and continuously displayed on a chart recorder.

The drive motor for the rods is a d.c. servo-motor‡ with a feed-back control system, which limits fluctuations in speed to less than 2 % under variable torque conditions. The operating speed range of the motor is approximately from 0·1 to 100 rev s^{-1}. The motor is mounted on a dove-tail slide, so that the rod is driven from above. The slide is attached to a steel support, which in turn is rigidly fastened to the steel table. This arrangement allows the initial insertion of the rod into the fluid to be made in a vertical direction.

Seven different aluminium rods were used in the experiments described in this paper. The radii of the rods are 0·079, 0·159, 0·317, 0·476, 0·635, 0·794 and 0·953 cm. With the exception of the smallest rod, each was carefully machined to ensure roundness along its full length, after which it was polished. The smallest rod was made from polished aluminium drill-rod. The upper end of each rod contains a tapered hole which fits a corresponding taper on the motor drive shaft. In this way, a rod can be attached concentrically to the motor drive shaft by means of a simple push fit. In addition, there is a small conical hole in the centre of the bottom of each rod, and this hole accepts the point of a spring-loaded cone bearing situated in the bottom of the fluid container. This method of aligning the rod proved to be very effective. For example, the largest rod

† By measuring the contact angle, we can accurately compute the height rise when $\Omega = 0$. The climbing constant $\hat{\beta}$ is selected so that the theoretical and measured rise curves have the same slope when $\Omega = 0$.

‡ Electrocraft Motomatic Type E-550.

showed less than 0·0013 cm eccentricity at any point along the rod when measured with a dial indicator.

The circular container for the fluid had a depth of 7·7 cm and a diameter of 30·5 cm, thus giving radius ratios of 16:1 and greater, so that the rod was effectively rotating in an infinite body of fluid. The container was accurately positioned on the table top by means of locating bars which allow the cone bearing in the bottom of the container to be aligned directly beneath the centre of the motor drive shaft.

Measurement of the rotational speed of the rod was accomplished by means of a small mirror attached to the motor drive shaft, a light source and photomultiplier tube, and a digital counter. This system was capable of measuring the rotational speed to within $\pm 0{\cdot}05$ rev s^{-1}.

Measurements of the shape of the free surface were made photographically using a two-camera technique. The cameras were mounted in front of the apparatus on a sliding horizontal track, so that their positions could be interchanged very rapidly. One camera was used to obtain a Polaroid slide of the shape of the free surface, and the other was used to obtain a positive–negative Polaroid print of the same shape. Both cameras were set to photograph at grazing incidence along the surface of the undisturbed liquid, which completely filled the liquid container. The Polaroid slides were later projected and quantitative measurements of the shape of the free surface were obtained from the enlarged images, using the known rod radius to establish the scaling factor. The Polaroid negatives were used to produce enlarged free-surface profiles, for comparison with theory in the method of profile fitting. Measurements made from these profiles also served as a check on the corresponding measurements from the slides. A further check on the height of climb of the liquid at the rod surface was provided by means of a direct reading using a cathetometer. The cathetometer was capable of discriminating to 0·005 cm, and the agreement between the scaled measurements and the cathetometer results indicated that the two methods have about the same accuracy.

When using the photographs and slides, it was necessary to be able to locate accurately the position of the free surface of the undisturbed liquid. This was accomplished by means of the two metal pointers shown on each side of the rod in figure 3. The pointers were positioned in a diametral plane normal to the direction from the camera to the rod. The vertical position of the pointers was carefully adjusted, so that the tips were as close to the surface of the liquid as possible, without actually touching it. In this way, the pointers and their reflexions in the surface of the liquid enabled the free surface in the plane of the pointers to be located.

It was important that the climbing data be obtained at successively greater values of the angular velocity, so that the height of climb at the rod surface never decreased. This avoided prior wetting of the rod surface by the liquid. The contact angle at the rod was hard to measure if the liquid was climbing on a rod which was coated with a thin film of the liquid.

8. Experiments with STP

Joseph *et al.* (1973) achieved good agreement between the theory of rod climbing and experiments with STP. But there were small discrepancies in the values of $\hat{\beta}$ that were of unclear origin. In addition, the method used to compute the static rise was, to a degree, *ad hoc*, and not perfectly matched to the basic theory. Our new experiments with STP were designed to clarify these two remaining areas of vagueness.

8.1. *Characterization of STP*

STP is a commercial motor oil additive. One of the effects of adding STP to motor oil is to increase the effective viscosity of the oil, and for this reason it is sometimes referred to as a viscosity index improver. It consists of a solution of polyisobutylene in a petroleum oil. We identified the polymer in a sample of the STP used for these experiments by first employing standard techniques to precipitate the polymer using methanol, then comparing an infra-red spectrograph of the precipitate with a standard spectrograph for polyisobutylene. All the STP used in these experiments came from the same production batch, for which the polymer content was 26·6 % by weight of the final product.

The density of the STP was measured as 0·89 g cm^{-3} at 20 °C, and was found to change by less than 1 % over a temperature range of 20–50 °C. The surface tension was measured using a standard ring tensiometer, and found to be 30·9 dynes cm^{-1}. The surface tension appeared not to vary with temperature over the range 20 °C to 50 °C. The normal and shear stresses were obtained as functions of the shear rate, using a rheometrics mechanical spectrometer. The shear stress and first normal stress difference are shown as functions of the shear rate in figure 4. From the former, it appears that STP has a nearly Newtonian shear viscosity. This is supported by the plot of shear viscosity as a function of shear rate shown in figure 5, which shows that the viscosity is virtually independent of shear rate at low rates of shear.

Two sets of data points are shown in figures 4 and 5. The solid points represent the results of tests with the cone and plate in a clean state, whereas the open points represent the results of tests of the same fluid at the same rates of shear using the cone and plate coated with Scotchgard. These results show that the Scotchgard has no apparent influence on the properties of the STP near the coated surfaces.

8.2. *The climbing of STP*

We turn now to a qualitative description of the sequence of changes in the free surface of the fluid near the rod as the speed of the rod is increased from zero. This sequence is depicted in figure 6 (plate 3), which shows a rod of 0·317 cm radius without the Scotchgard surface coating. When the rod is at rest, the climb is due entirely to wetting at the surface. As the rotational speed is increased to about 3 rev s^{-1}, the liquid climbs the rod. The initially concave shape of the free surface of the climbing fluid gradually assumes a slightly convex form. It is in this speed range (0 to about 3 rev s^{-1}) that the second-order theory is in good agreement with experimental results. As the speed is increased further,

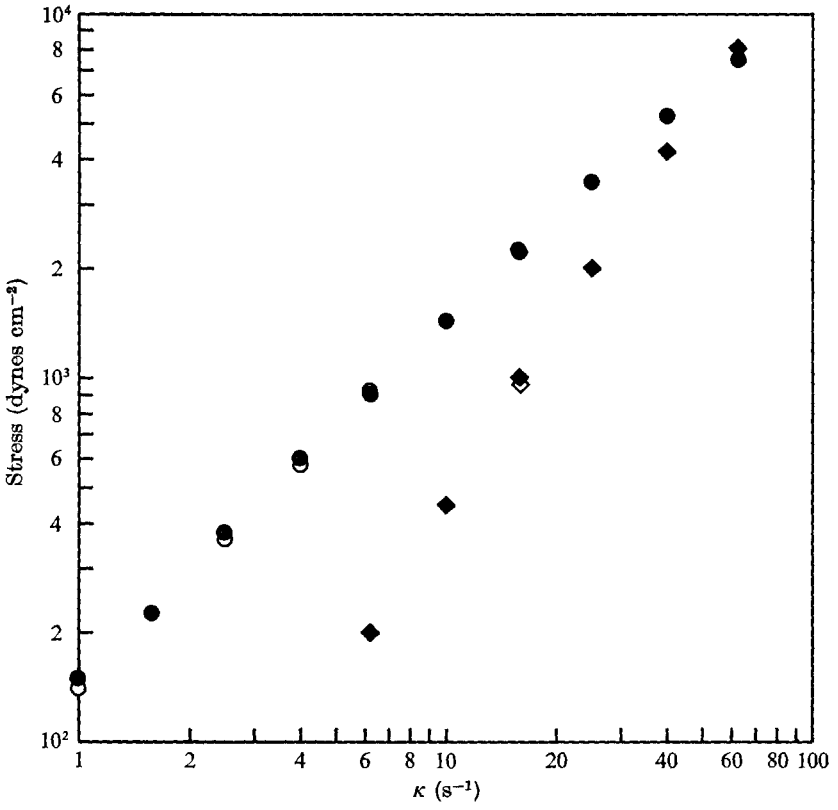

FIGURE 4. Shear stress and first normal stress difference of STP as functions of shear rate. All stresses and shear rates were measured both with and without the cone and plate coated with Scotchgard.

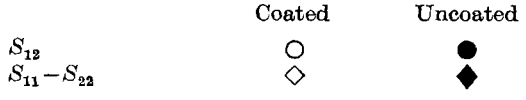

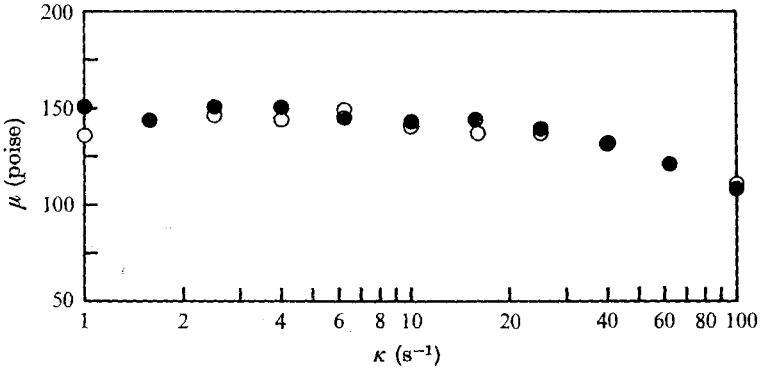

FIGURE 5. Shear viscosity of STP as a function of shear rate: ○, cone and plate coated with Scotchgard; ●, uncoated.

the free surface becomes more convex as secondary motions within the climbing fluid become important. The final stable configuration assumed by the drop of climbing fluid before instability is shown in photograph (*h*) of figure 6. The fluid appears to meet the main body of fluid at a point of discontinuity of slope; close inspection reveals a smooth but very rapid variation.

At larger values of the rotational speed the steady droplike configuration loses its stability to a time-periodic motion which first appears with only infinitesimal amplitude. The time-periodic motion is a bifurcating flow whose amplitude increases with speed. In the time-periodic motion, a band of fluid appears to rise slowly almost to the full height to which the fluid climbs up the rod, then to collapse downwards to the main body of fluid. The periodic motion is very regular, and increases in frequency as the rotational speed is increased. Figure 7 (plate 4) shows the motion for one complete cycle for a rod rotating at 13·3 rev s^{-1}; the frequency of the periodic motion is 0·4 cycles s^{-1}. Finally, when the rotational speed is increased further, the free surface ruptures, and globules of fluid are thrown away from the oscillating drop.

8.3. *Experiments at room temperature when the STP wets the rod*

In these experiments we rotated each of seven available rods in STP at room temperature (about 26 °C). The rods were not coated with Scotchgard, and there was always a rise due to wetting, with wetting angles of about 45°. The plots of $h(a;\omega^2)$ against ω^2 are similar to those of Joseph *et al.* (1973), and to the samples given in figure 8. This figure shows height-rise graphs for the same rod at three different temperatures. It is clear that the height of climb at the rod is greatly influenced by the temperature of the fluid (see §8.5). The three plots, however, exhibit the same general features. The height-rise curve $h(a;\omega^2)$ is linear when ω is small, is convex at all ω, and reaches a nearly constant value before instability.

Experimental values of $h(a;\omega^2)$ at small ω^2 for each of the seven rods are shown in figure 9. The height of climb at each rod appears to be linear in ω^2 for values of ω^2 less than about 12. The slopes of the linear regions were found using a least-squares fit, and the associated values of $\hat{\beta}$ are listed in table 1. These results, all obtained at approximately the same temperature, show very little scatter. At a given temperature, there is no dependence of $\hat{\beta}$ upon the rod radius.

The method of profile fitting was used to check the values of $\hat{\beta}$ found by the method of slopes. Predicted and measured profiles were compared at four different rotational speeds between about 1 rev s^{-1} and 3 rev s^{-1} for each of the rods. The comparisons for six of the rods are given in figure 10. The second-order theory gives accurate predictions of the free-surface shape when the value of $\hat{\beta}$ is determined by the method of slopes. For these experiments, in which the linear portion of the height-rise curve is well defined, the method of slopes can be used to determine an accurate value for $\hat{\beta}$, from which we can predict accurately the shape of the free surface. For fluids that have a smaller range of ω^2 in which second-order theory holds (like polyacrylamide), the determination of $\hat{\beta}$ is most accurately accomplished by means of the method of profile fitting (see §9).

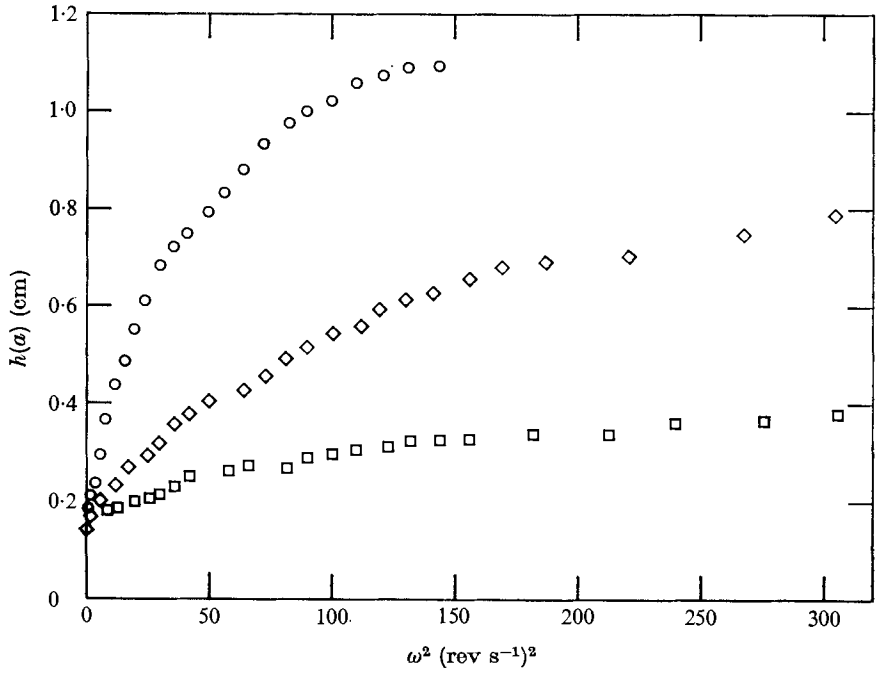

FIGURE 8. Typical plots of $h(a;\omega^2)$ against ω^2 for an uncoated rod (radius a = 0·317 cm) in STP at different temperatures.

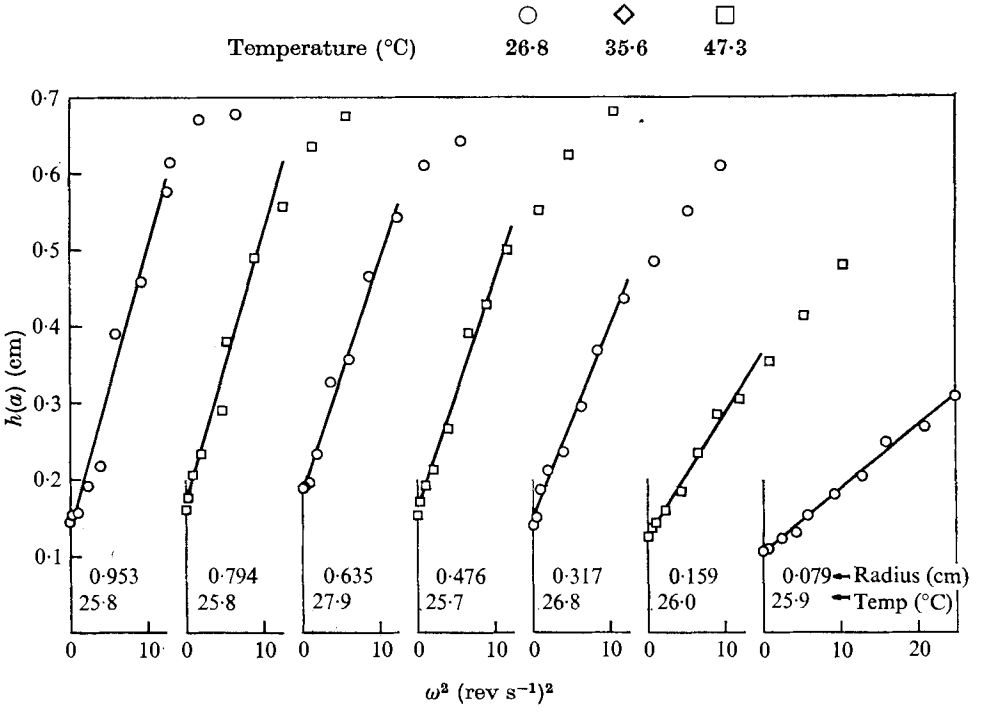

FIGURE 9. Experimental values of $h(a;\omega^2)$ at small ω^2 for seven uncoated rods in STP at room temperature.

Rod radius (cm)	Temperature (°C)	$\hat{\beta}$ (g cm^{-1})
0·079	25·9	0·96
0·159	26·0	1·02
0·317	26·8	0·97
0·476	25·7	0·93
0·635	27·9	0·86
0·794	25·8	0·95
0·953	25·8	1·00

TABLE 1. Values of $\hat{\beta}$ for STP near room temperature.
In these experiments the rod was not coated and the STP wet the rod

8.4. *Experiments at room temperature when the rods are coated with Scotchgard*

When the free surface of the fluid does not make perpendicular contact with the rod it is necessary to specify the slope of the fluid surface at the rod, to compute profiles for the method of profile fitting. The theory assumes perpendicular contact at the rod. When the contact is not perpendicular, a static rise is added to that computed from theory. The static rise is computed from the surface-tension equation with the value of the prescribed contact angle taken from the experimental profiles. The computed climb due to wetting is quite sensitive to the value of the contact angle, which must therefore be measured accurately from the experimental profiles. By coating the rods with Scotchgard, we were able to achieve a zero slope at the rod surface. This eliminates the need for a correction for the static rise, and matches perfectly in the experiments the conditions assumed in the analysis.

The flatness of the contact between the STP and the rod is apparent in the photographs of figure 11 (plate 5). When the rod is stationary (figure 11(*a*)) no static climb is observed. As the rotational speed is increased, the STP climbs up the rod, maintaining a flat contact with the rod. The surface profiles are somewhat similar to those shown in figure 6, except very close to the rod, where the wetting has a strong influence on the profile. The apparent wavelike shape that appears in the profiles of figure 11 for the higher velocities is an optical effect, which arises from the lighting arrangement. The top of the STP drop is flat and smooth; light reflected from the upper part of the rod on to the surface of the drop gives the impression that the liquid surface has a wavelike character.

Surface profiles were measured on STP for three rods coated with Scotchgard, using the photographic techniques. In addition, a cathetometer was used to check the rise at the rod. The quantity $h(a;\omega^2)$ is plotted as a function of ω^2 for each rod in figure 12. The values of $\hat{\beta}$ found from the slopes of the linear portions of the curves obtained from the experiments with coated and uncoated rods were consistent with one another. The two sets of results are compared in figure 15. The free-surface profiles computed from (4.16) are in excellent agreement with the measured profiles for the coated rods (figure 13) for rotational speeds up to about 3 rev s^{-1}.

The two plots in the upper part of figure 12 show the results of a test carried out to substantiate the earlier finding that the Scotchgard had no effect on the

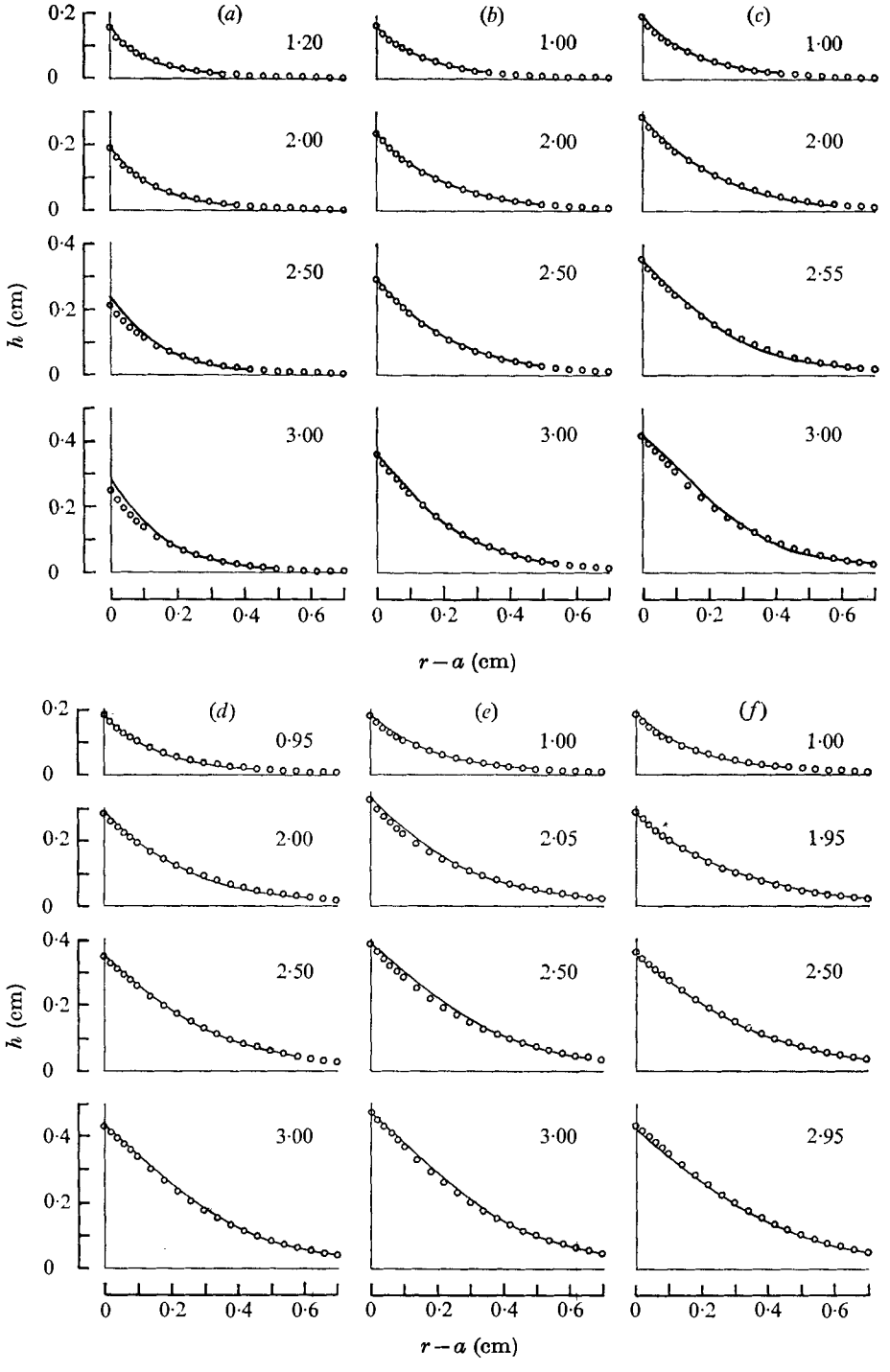

FIGURE 10. Profile fitting for STP at room temperature. Comparison of observed with predicted profiles, for uncoated rods. Comparisons identified by rod rotational speed (rev s^{-1}).

	(a)	(b)	(c)	(d)	(e)	(f)
a (cm)	0·159	0·317	0·476	0·635	0·794	0·953

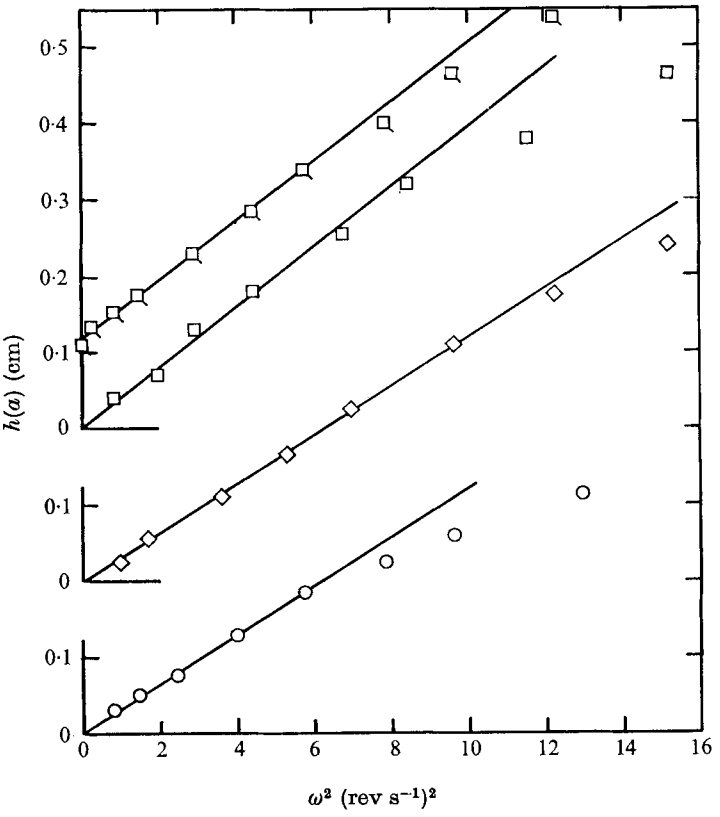

FIGURE 12. Experimental values of $h(a;\omega^2)$ at small ω^2, for rods coated and uncoated with Scotchgard, in STP at room temperature.

	Uncoated	Coated		
a (cm)	0·635	0·635	0·476	0·317

STP near the rod. We first rotated a clean rod (radius 0·635 cm) in STP, then we coated the rod with Scotchgard and rotated it again. The slopes of the plots of $h(a;\omega^2)$ against ω^2 are identical; the difference in the actual rise is constant and equal to the static rise.

8.5. *The effects of varying the temperature*

The discrepancies in the values reported for $\hat{\beta}$ in Joseph *et al.* (1973) suggested that small changes in temperature may cause appreciable changes in the value of $\hat{\beta}$. The results presented here allow us to make this conjecture precise.

The influence of temperature on the climb of STP is emphatically demonstrated in the photographs of figure 14 (plate 6). These show the same rod (radius 0·476 cm) rotating at the same speed (5 rev s^{-1}) in the same batch of STP, the only difference being in the temperature of the fluid, which is 46·1, 25·6 and 5·0 °C in (*a*), (*b*) and (*c*), respectively. The differences in the rise are dramatic: the rise at the rod at

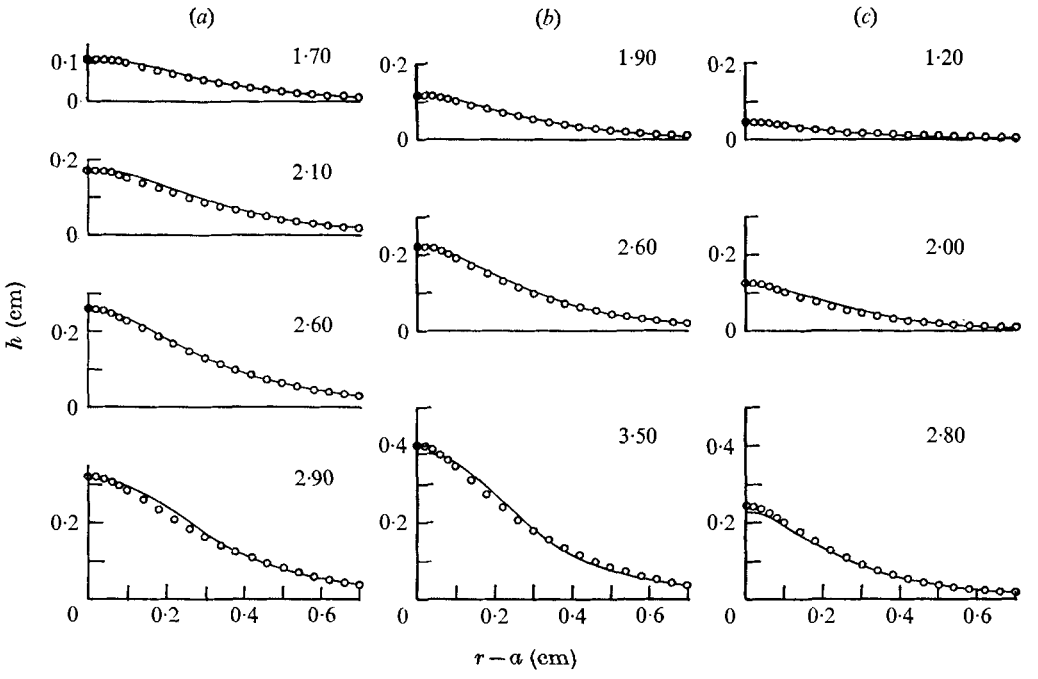

FIGURE 13. Profile fitting for STP at room temperature. Comparison of observed with predicted profiles, for three rods coated with Scotchgard. Comparisons identified by rod speed (rev s^{-1}).

	(a)	(b)	(c)
a (cm)	0·635	0·476	0·317

5·0 °C is almost ten times the value at 46·1 °C. There are correspondingly large differences in the values of $\hat{\beta}$. The approximate solution (4.19) to (4.16) for the climb at second order shows that, for a given radius and rotational speed, the climb at the rod increases linearly with $\hat{\beta}$. Thus, the photographs of figure 14 indicate that, as the temperature is increased, a large decrease is to be expected in the value of $\hat{\beta}$.

Quantitative measurements of $\hat{\beta}$ were made at temperatures in the range from about 25 to 50 °C, using uncoated rods. The variation of $\hat{\beta}$ with temperature is shown in figure 15. It is evident that $\hat{\beta}$ depends strongly on the temperature; it changes by a factor of ten over the range of temperatures covered in figure 15. By curve fitting, we find that

$$\hat{\beta} = 20\exp(-0{\cdot}115T)\ \text{g cm}^{-1}, \quad 25\ ^{\circ}\text{C} < T < 50\ ^{\circ}\text{C}. \tag{8.1}$$

Equation (8.1) is probably the only known empirical formula giving the temperature dependence of a Rivlin–Ericksen constant, other than the viscosity. It shows how important it is to control the temperature in experiments to determine the values of the Rivlin–Ericksen constants. Insufficient attention was paid to temperature in the Joseph *et al.* (1973) experiments; daily temperature variations of over 2 °C in the laboratory are more than sufficient to produce a 20 % discrepancy in $\hat{\beta}$.

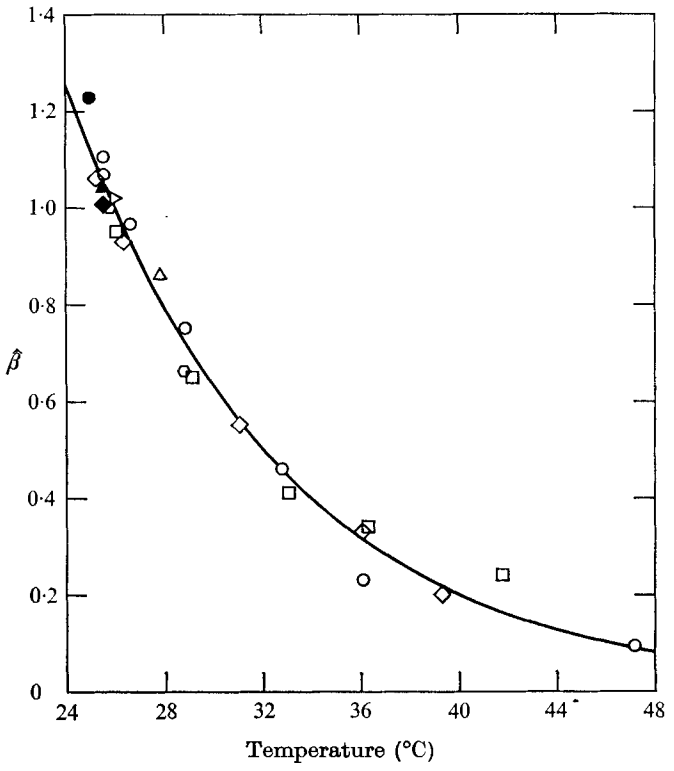

FIGURE 15. Variation of $\hat{\beta}$ (g cm^{-1}) with temperature (°C), for STP. ——, empirical relation $\hat{\beta} = 20 \exp(-0{\cdot}115\,T)$, $25 < T < 50$ °C.

Coated	●	◆	▲			
Uncoated	▷	○	◇	△	□	○
a (cm)	0·159	0·317	0·476	0·635	0·794	0·953

The effect of increasing rotational speed on the free surface at a temperature of 46·1 °C is shown in the sequence of photographs of figure 16 (plate 7). The rise of the fluid at 46·1 °C (rod radius 0·476 cm) is stable at much higher rotational speeds than at 25 °C (compare figures 16 and 6). As the rotational speed is increased to very high values, the rise decreases, and is eventually replaced with an inertia-dominated depression of the free surface (figure 16(*h*)). The depression of the free surface at high speeds may be caused by viscous heating due to the high rates of shear near the rod.

It is interesting to note that we were able completely to eliminate the climb on this rod at all rotational speeds, by raising the fluid temperature to 56 °C. At this temperature, the free surface of the fluid sinks, as it does for the Newtonian oil in figure 1. These observations are consistent with the notion of a critical radius (equation (4.17)). The critical radius, based on the value given by (8.1) at 56 °C, is about 0·38 cm; the rod radius is 0·476 cm, and the fluid cannot climb.

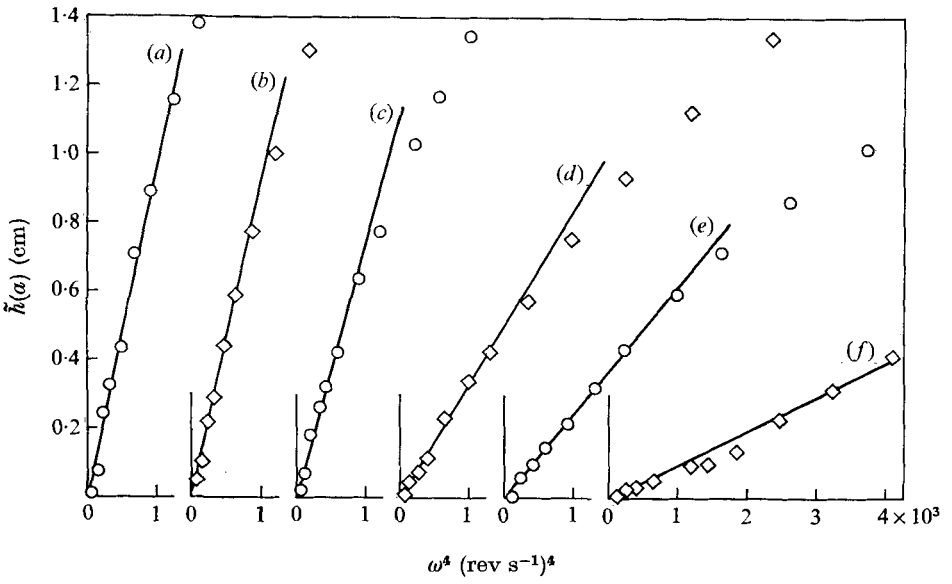

FIGURE 17. Residual $\tilde{h}$ as a function of ω^4 for uncoated rods, rotating in STP at room temperature.

	(*a*)	(*b*)	(*c*)	(*d*)	(*e*)	(*f*)
a (cm)	0·953	0·794	0·635	0·476	0·317	0·159

8.6. *Rod climbing at higher orders*

The experiments described in Joseph *et al.* (1973) and here are compared with the second-order theory. Both sets of experiments show that the range of rotational speeds for which the second-order theory holds is in the interval of ω from 0 to about 3 rev s^{-1}. To investigate rod climbing at higher orders, we adopted the following procedure: we computed $\hat{\beta}$ from the second-order theory, then we defined a residual $\tilde{h}$ as

$$-\tilde{h} = h(a;\omega^2)_{\exp} - h_s - h^{\langle 2\rangle} 4\pi^2\omega^2,$$

where $h^{\langle 2\rangle}$ is given by (4.19). The residual gives the remainder of the height rise after terms $O(\omega^2)$; given a series representation in powers of ω^2, the residual is $O(\omega^4)$. In figure 17 we have plotted the residual as a function of ω^4 for the experiments from which figure 9 was prepared. The residual for each rod is linear over a substantial portion of the rise curve (up to about 6 rev s^{-1}). This suggests that STP, in this speed range, may be fairly well modelled by a fluid of grade four. We are going to investigate this interesting possibility in the course of our planned efforts to obtain the values of the Rivlin–Ericksen constants up to order four from the rotating rod viscometer.

9. Experiments with polyacrylamide

The results, presented in Joseph *et al.* (1973) and §8, leave open the possibility that the second-order theory of Joseph & Fosdick (1973) and Joseph *et al.* (1973) can be applied only to STP. To test the second-order theory with a second

common fluid, we performed a series of experiments using a solution of polyacrylamide powder in a glycerine–water mixture. This fluid was chosen because it is known that the dependence of the shear viscosity on the shear rate is quite different from that of STP (polyacrylamide possesses pseudoplastic characteristics).

A solution containing 1·48 % by weight of polyacrylamide powder was manufactured as follows: 6·492 kg glycerine, 6·492 kg distilled water, 0·195 kg polyacrylamide powder.† The glycerine and water were thoroughly mixed, then the powder was added very slowly by passing it through a flour sifter into the vortex formed by a rotating stirrer. The powder was added to the solution over a period of several hours, after which the solution was allowed to sit for several days.

A specific gravity bottle was used to determine the density as 1·21 g cm^{-3} at 24·1 °C. The surface tension of the fluid was measured using a standard ring tensiometer. The response of the polyacrylamide surface to the ring tensiometer is viscoelastic and is not like STP. Classical surface tension seems inadequate to explain surface behaviour at an air–polyacrylamide surface. Our measurements of surface tension were made several times over time intervals of several minutes each, and the resulting value for the surface tension was found to be 58 dynes cm^{-1}. These values for the density and surface tension were used in the numerical computations for both the method of slopes and the method of profile fitting.

9.1. *Experiments at room temperature*

In all these experiments, the static climb was eliminated by coating the rods with Scotchgard. The first experiments were performed at room temperature a few days after the fluid had been mixed. Four different rods (a = 0·317, 0·476, 0·635 and 0·794 cm) were used in the viscometer. The procedure was the same as that used for the STP; the measurements (both from the slides and with the cathetometer) were a little more difficult, because polyacrylamide is optically transparent.

The plots of the height of climb at the rod as functions of ω^2 are shown in figure 18 for the four rods. Comparison with figure 9 shows that the apparent region of linearity is less for the polyacrylamide solution than for STP. Thus, to obtain the best possible values for $\hat{\beta}$ from the data, it was decided to use profile fitting, and seek values for $\hat{\beta}$ that would match experimental and calculated profiles at the lowest angular velocities for which distinct profiles could be measured. The values of $\hat{\beta}$ obtained in this way were then used to compare profiles at other angular velocities up to about 3·5 rev s^{-1} for each rod. The values obtained for $\hat{\beta}$ are given in table 2, and the corresponding profile comparisons are shown in figure 19. In addition, the values of $\hat{\beta}$ were used to compute the slope

$$dh(a;\omega^2)/d\omega^2$$

for each rod, and these are the lines shown in figure 18. They are good representations of the data for values of ω^2 less than about six.

† Type Cyanamer P-250, manufactured by the American Cyanamid Company.

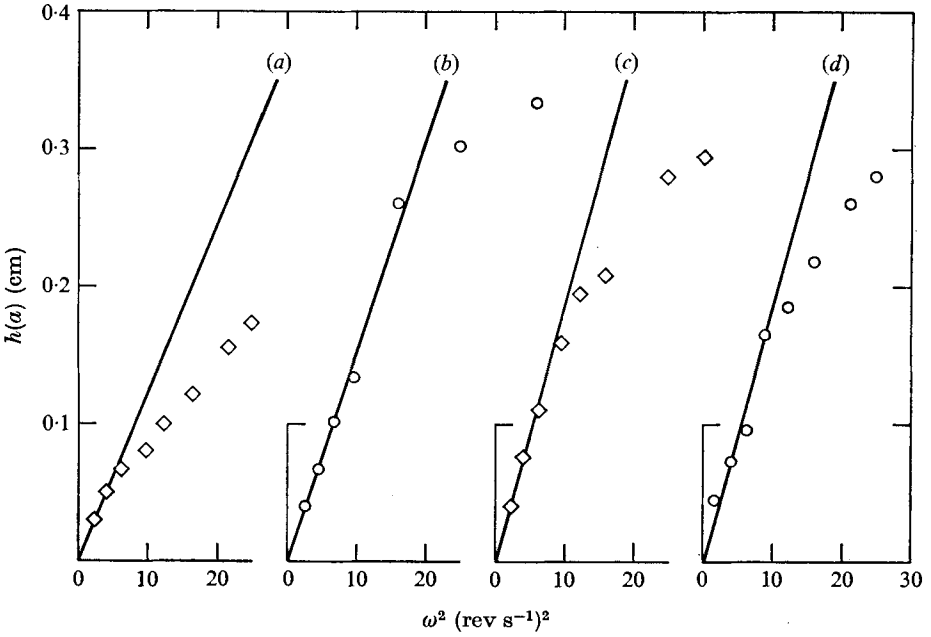

FIGURE 18. Experimental values of $h(a;\omega^2)$ at small ω^2 for rods coated with Scotchgard, rotating in polyacrylamide solution at approximately 24 °C (see table 2). Slopes of lines are determined using values of $\hat{\beta}$ obtained by the method of profile fitting (figure 19).

	(*a*)	(*b*)	(*c*)	(*d*)
a (cm)	0·317	0·476	0·635	0·794

9.2. *The effects of varying the temperature*

Following the procedure used for STP, an attempt was made to investigate the influence of temperature on the value of $\hat{\beta}$. Unfortunately it was not possible to obtain a graph showing the dependence of $\hat{\beta}$ upon temperature, owing to the unexpected behaviour of the fluid at temperatures above room temperature. These effects will be summarized below.

When the speed of rotation of the rod was increased at room temperature, the shape of the free surface was similar to those shown in figure 11. The rise did not increase much with the angular velocity at large values of the angular velocity; it appeared rapidly to approach a constant maximum value, but before this value was attained the steady configuration was destroyed by instabilities. The critical speed for instability is much higher in polyacrylamide than in STP, and the time-periodic flow itself is very unstable in polyacrylamide.

The behaviour of polyacrylamide at high temperatures is unlike polyacrylamide at room temperature or STP at any temperature in the range $25 < T < 50$ °C. This difference is made clear in figure 20 (plate 8). The figure shows a rod of radius 0·476 cm rotating in the polyacrylamide solution at a temperature of 38·3 °C, for angular velocities between 1 and 70·0 rev s^{-1}. At 1·0 rev s^{-1} the free surface is already beginning to assume the bell-shaped profile distinctive of profiles for which the second-order theory is not adequate to describe the motion.

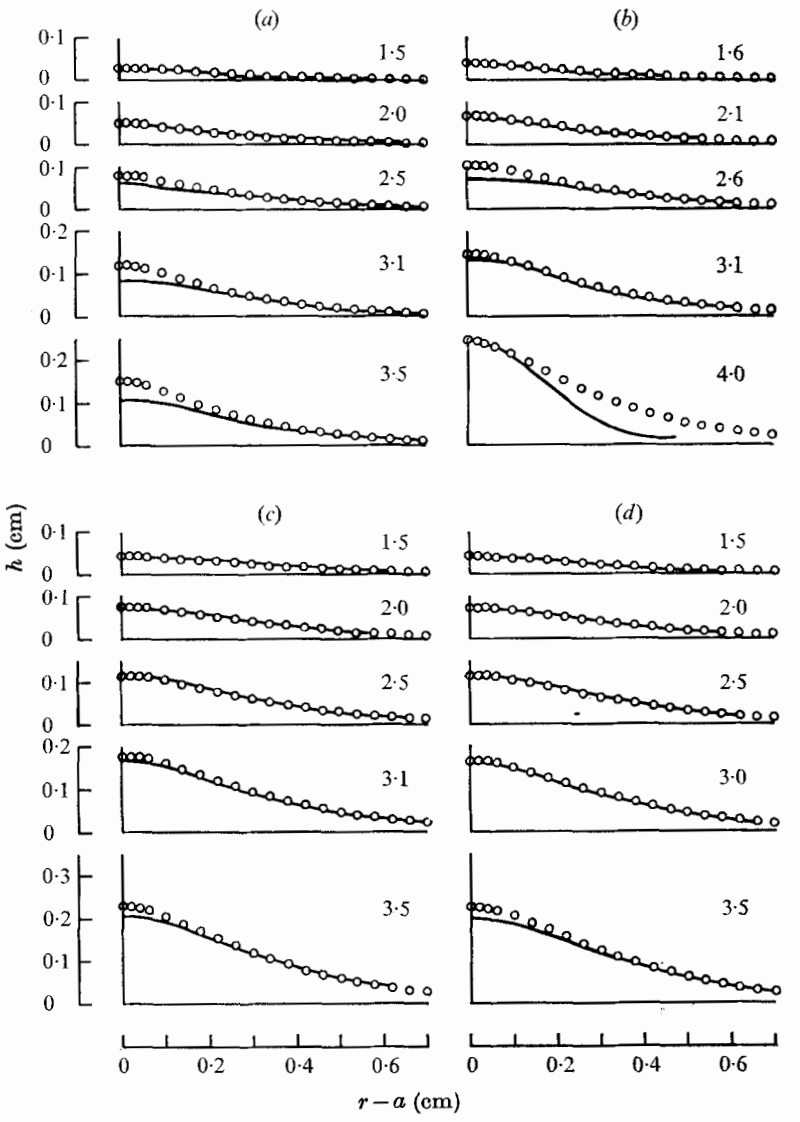

FIGURE 19. Profile fitting for polyacrylamide solution. Comparison of observed with predicted profiles for lowest rotational speeds of figure 18.

	(a)	(b)	(c)	(d)
a (cm)	0·317	0·476	0·635	0·794

At 2·5 rev s^{-1} (figure 20(*b*)) and 5·5 rev s^{-1} (figure 20(*c*)), the bell-shaped profile continues to grow, reaching a maximum height eventually at about 25 rev s^{-1} (figure 20(*d*)). As the speed is further increased, the fluid tends to spread radially and the height of climb at the rod starts to decrease, as shown in figure 20(*e*) at 45 rev s^{-1}. This trend continues up to about 70 rev s^{-1} (figure 20(*f*)), at which speed the drop of climbing fluid broke up.

The absence of any measurable linear region on a plot of $h(a;\omega^2)$ against ω^2

Rod radius (cm)	Temperature (°C)	$\hat{\beta}$ (g cm^{-1})
0·317	24·4	0·78
0·476	23·9	0·76
0·635	24·2	0·84
0·794	24·4	0·84

TABLE 2. Values of the climbing constant for a fresh solution of polyacrylamide (1·48%) in glycerine and water

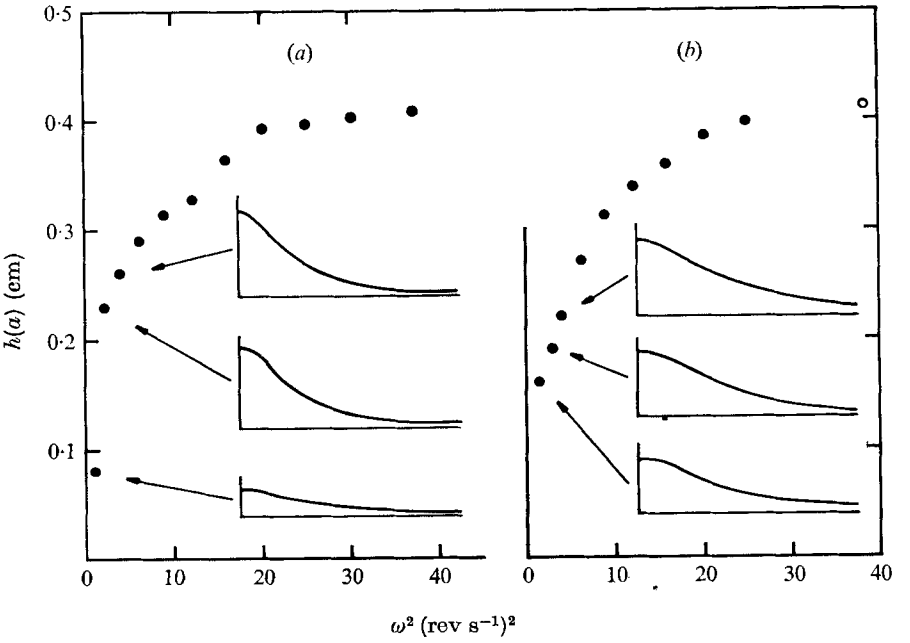

FIGURE 21. Experimental values of $h(a;\omega^2)$ for rods coated with Scotchgard, rotating in polyacrylamide. No measurable linear region. Observed profile shapes for lowest rotational speeds are similar to profile shapes at much higher speeds when temperature is lower.

	a (cm)	Temperature (°C)
(*a*)	0·476	38·3
(*b*)	0·635	33·1

at higher temperatures is clearly shown in figure 21, which presents data for the 0·476 cm radius rod at 38·3 °C and the 0·635 cm radius rod at a temperature of 33·1 °C. Also shown in this figure are sketches made from enlarged tracings of the actual profiles for the three lowest angular velocities at which a clear profile could be discerned. The profiles have shapes very similar to the profile shapes obtained at much higher angular velocities when the temperature is lower. No value of $\hat{\beta}$ could be determined by either the method of slopes or the method of profile fitting. This determination will require consideration of terms arising in the higher-order theory.

After the experiments at 38·3 and 33·1 °C, the liquid was allowed to cool to room temperature (24·4 °C), and another experimental run was made using the

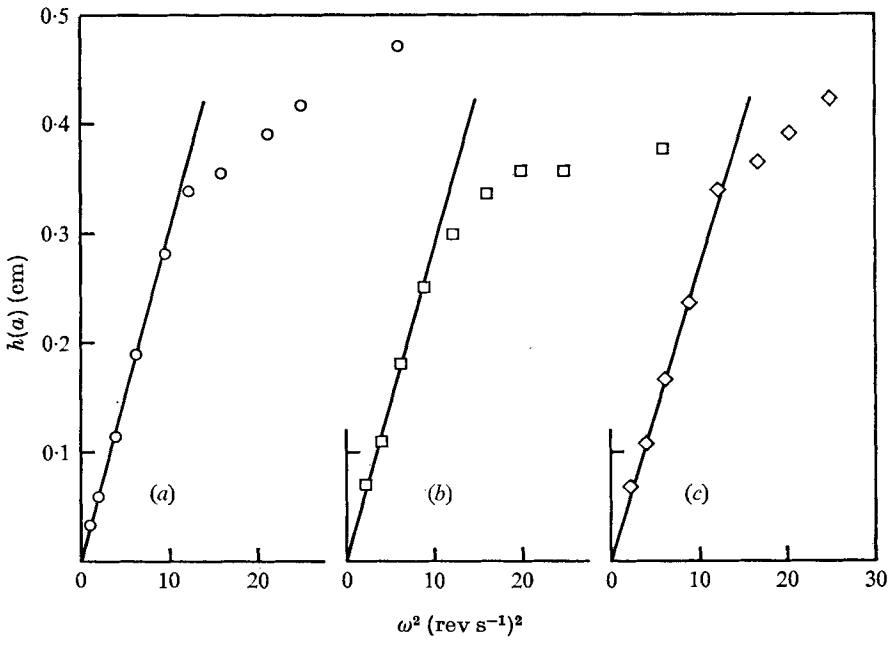

FIGURE 22. Experimental values of $h(a;\omega^2)$ at small ω^2 for one rod (radius $a = 0{\cdot}476$ cm) coated with Scotchgard, rotating in polyacrylamide, after heating and subsequent cooling of the fluid.

	(a)	(b)	(c)
Temperature (°C)	24·4	24·4	27·2

0·476 cm rod. In this instance, there was a definite linear region for $\omega^2 < 10$ (figure 22(*a*)), and the method of slopes and method of profile fitting could both be used to obtain the value $\hat{\beta} = 1{\cdot}4$ g cm^{-1}, a value considerably greater than that obtained earlier at the same temperature. Further heating and cooling produced similar effects, so that it would appear that the initial heating of the fluid changed it in some way.

A complete description of the experiments with the polyacrylamide solution is given, with the experiments listed in chronological order. (i) Soon after the liquid was mixed, experiments at room temperature were performed with four different rods. The resulting values of $\hat{\beta}$ are given in table 2. (ii) The liquid was allowed to stand in a covered container for one week, then the 0·476 cm rod was used. $\hat{\beta}$ was found to be 0·74 g cm^{-1} at 22·8 °C. (iii) The liquid was heated to 38·3 °C. No value of $\hat{\beta}$ could be found, because of the apparent lack of a measurable range of ω in which second-order theory is adequate (figure 21). (iv) The liquid was cooled to 33·1 °C. Again, no value of $\hat{\beta}$ could be found (figure 21). (v) The liquid was cooled to 24·4 °C, and $\hat{\beta}$ was obtained as 1·40 g cm^{-1} (figure 22(*a*)). (vi) The liquid was left in a covered container for two weeks, then the experiment at 24·4 °C was repeated. The value for $\hat{\beta}$ was found to be 1·6 g cm^{-1}. (vii) The liquid was heated to 35·6 °C. No value of $\hat{\beta}$ could be found. (viii) The liquid was then cooled to 24·4 °C, and again the method of slopes and the method of profile fitting could be applied, giving a value for $\hat{\beta}$ of 1·36 g cm^{-1} (figure 22(*b*)). (ix) The

liquid was next heated to 27·2 °C; and it was again possible to determine a value for $\hat{\beta}$ ($\hat{\beta} = 1{\cdot}26\,\mathrm{g\,cm^{-1}}$: figure 22(*c*)).

From these experiments, it is concluded that the second-order theory can be used for polyacrylamide solutions of the type used in this project, provided the temperature is such that there is a discernible range of rod speeds for which $h(a;\omega^2)$ is linearly proportional to ω^2. For the solution used in these experiments, this linear region existed when the temperature of the fluid was less than about 28 °C. The large difference in the values obtained for $\hat{\beta}$ before and after heating is caused by permanent heat-induced changes in the polyacrylamide.

We gratefully acknowledge the assistance of C. G. Trowbridge in all aspects of the experimental programme. Our work was supported in part under grants GK-37675 and GK-12500 from the National Science Foundation.

REFERENCES

COLEMAN, B. D., MARKOVITZ, H. & NOLL, W. 1966 *Viscometric Flows of Non-Newtonian Fluids. Springer Tracts in Natural Philosophy*, vol. 5. Springer.

COLEMAN, B. D. & NOLL, W. 1960 An approximation theorem for functions with applications in continuum mechanics. *Arch. Rat. Mech. Anal.* **6**, 355.

COLEMAN, B. D. & NOLL, W. 1961 Foundations of linear visco-elasticity. *Rev. Modern Phys.* **33**, 239.

GIESEKUS, VON H. 1961 Einige Bemerkungen zum Fließverhalten elasto-viskoser Flüssigkeiten in stationären Schichtströmungen. *Rheologica Acta*, **1**, 404.

JOSEPH, D. D. 1973 Domain perturbations: the higher order theory of infinitesimal water waves. *Arch. Rat. Mech. Anal.* **51**, 295.

JOSEPH, D. D., BEAVERS, G. S. & FOSDICK, R. L. 1973 The free surface on a liquid between cylinders rotating at different speeds. Part 2. *Arch. Rat. Mech. Anal.* **49**, 381.

JOSEPH, D. D. & FOSDICK, R. L. 1973 The free surface on a liquid between cylinders rotating at different speeds. Part 1. *Arch. Rat. Mech. Anal.* **49**, 321.

JOSEPH, D. D. & STURGES, L. 1975 The free surface on a liquid in a trench heated from its side. *J. Fluid Mech.* **69**, 565.

LANGLOIS, W. E. & RIVLIN, R. S. 1963 Slow steady-state flow of visco-elastic fluids through non-circular tubes. *Rendiconti di Matematica*, **22**, 169.

MARKOVITZ, H. & COLEMAN, B. D. 1964 Incompressible second-order fluids. *Advances in Applied Mechanics*, vol. 8. Academic.

NOLL, W. 1958 A mathematical theory of the mechanical behaviour of continuous media. *Arch. Rat. Mech. Anal.* **2**, 197.

PIPKIN, A. C. & TANNER, R. I. 1973 A survey of theory and experiment in viscometric flows of viscoelastic liquids. *Mechanics Today*, vol. 1. Pergamon.

PRITCHARD, W. G. 1971 Measurements of the viscometric functions for a fluid in steady shear flow. *Phil. Trans.* A **270**, 507.

SERRIN, J. 1959 Poiseuille and Couette flow of non-Newtonian fluids. *Z. angew. Math. Mech.* **39**, 295.

TANNER, R. I. 1970 Some methods for estimating the normal stress functions in viscometric flows. *Trans. Soc. Rheol.* **14**, 483.

TRUESDELL, C. 1974 The meaning of viscometry in fluid dynamics. *Annual Reviews of Fluid Mechanics*, vol. 6. Annual Reviews Inc.

TRUESDELL, C. & NOLL, W. 1965 The nonlinear field theories of mechanics. *Handbuch der Physik*, vol. III/3. Springer.

WINEMAN, A. S. & PIPKIN, A. C. 1966 Slow viscoelastic flow in tilted troughs. *Acta Mechanica*, **2**, 104.

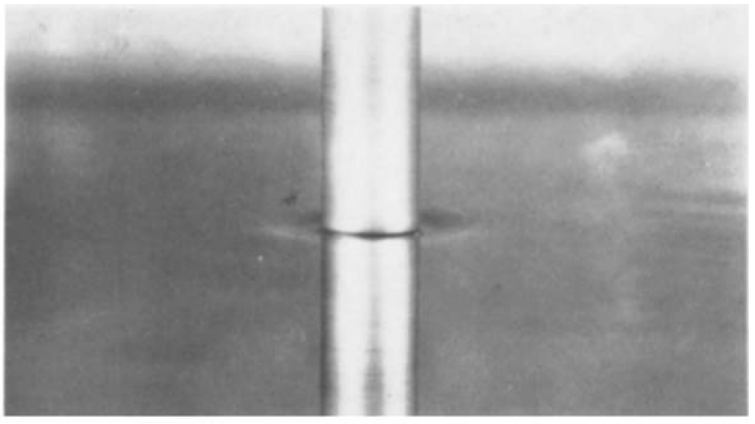

(*a*)

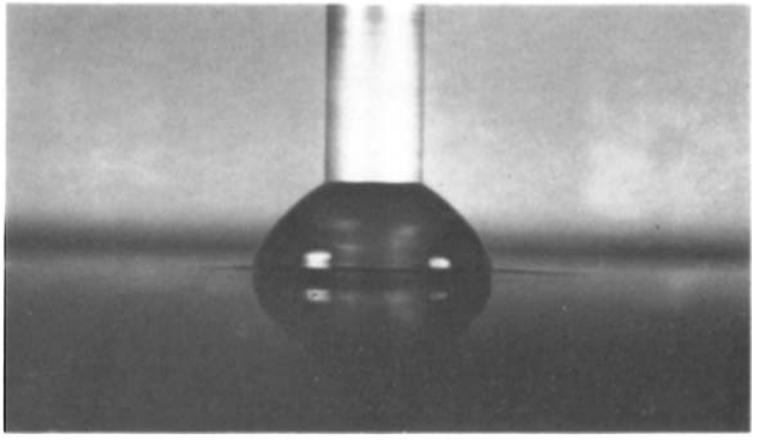

(*b*)

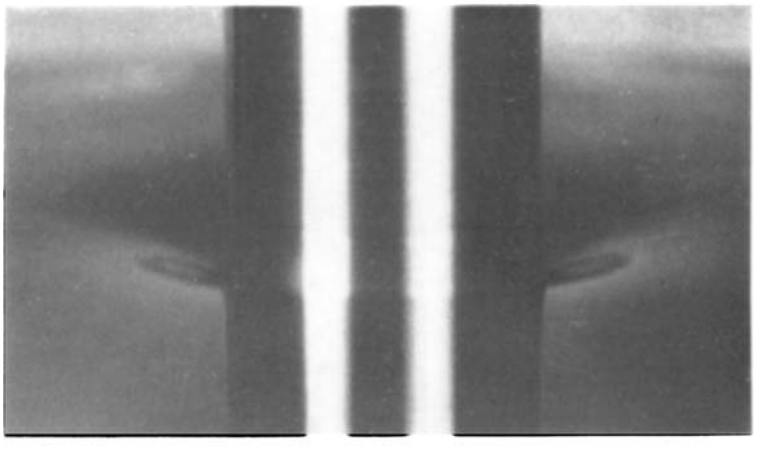

(*c*)

FIGURE 1. Rods rotating at 10 rev s^{-1}.

		Rod radius (cm)	Temperature (°C)	$\hat{\beta}$ (g cm^{-1})	Fluid near rod
(*a*)	In Newtonian oil (Sinclair 100 Duro)	0·476	25·0	—	Sinks
(*b*)	In STP motor oil additive	0·476	26·0	0·98	Climbs
(*c*)	In STP motor oil additive	1·905	28·5	0·76	Cannot climb

(*Facing p.* 512)

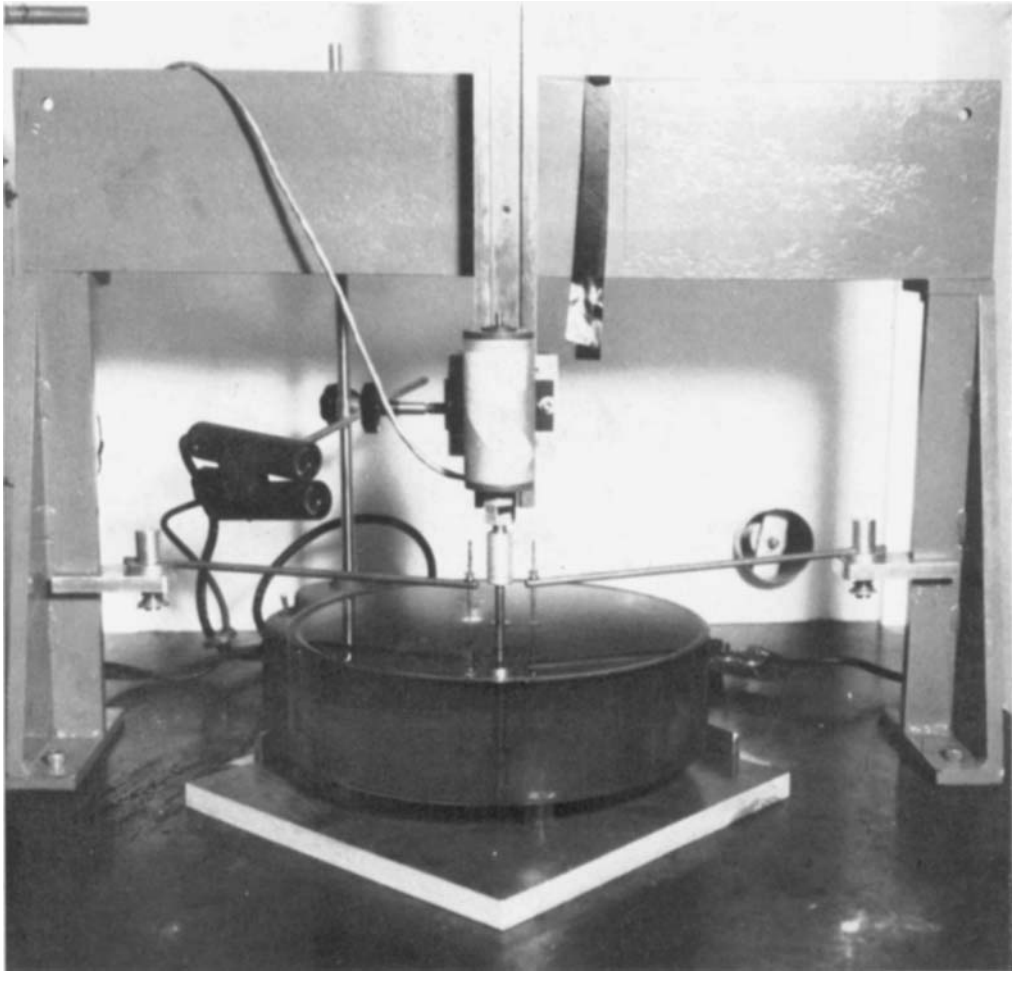

FIGURE 3. Apparatus.

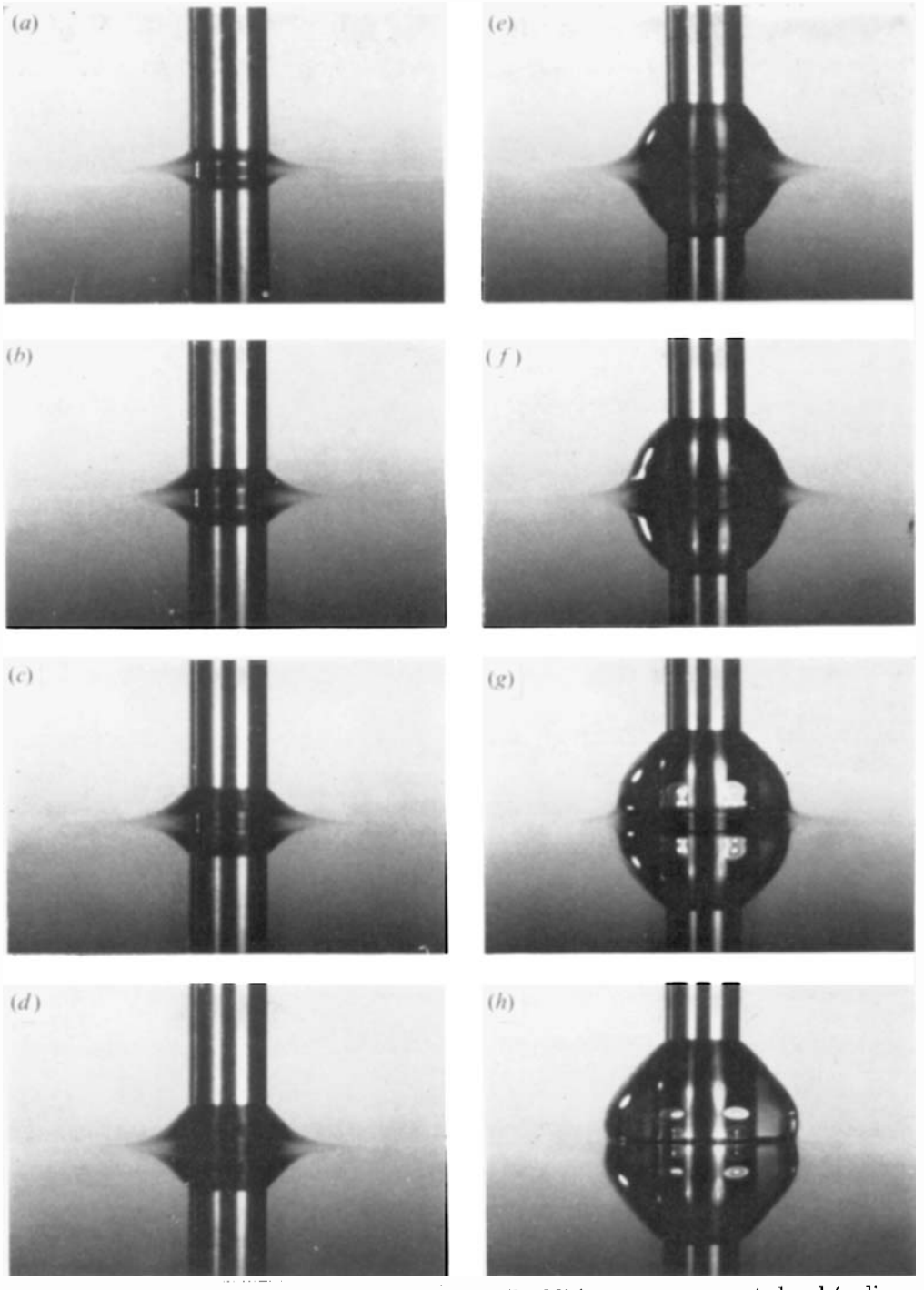

FIGURE 6. Change in free surface of STP motor oil additive near an uncoated rod (radius $a = 0{\cdot}317$ cm) as rotational speed is increased; temperature, 26·7 °C.

	(*a*)	(*b*)	(*c*)	(*d*)	(*e*)	(*f*)	(*g*)	(*h*)
Speed (rev s^{-1})	1·0	2·0	2·5	3·0	4·6	5·5	7·0	8·5

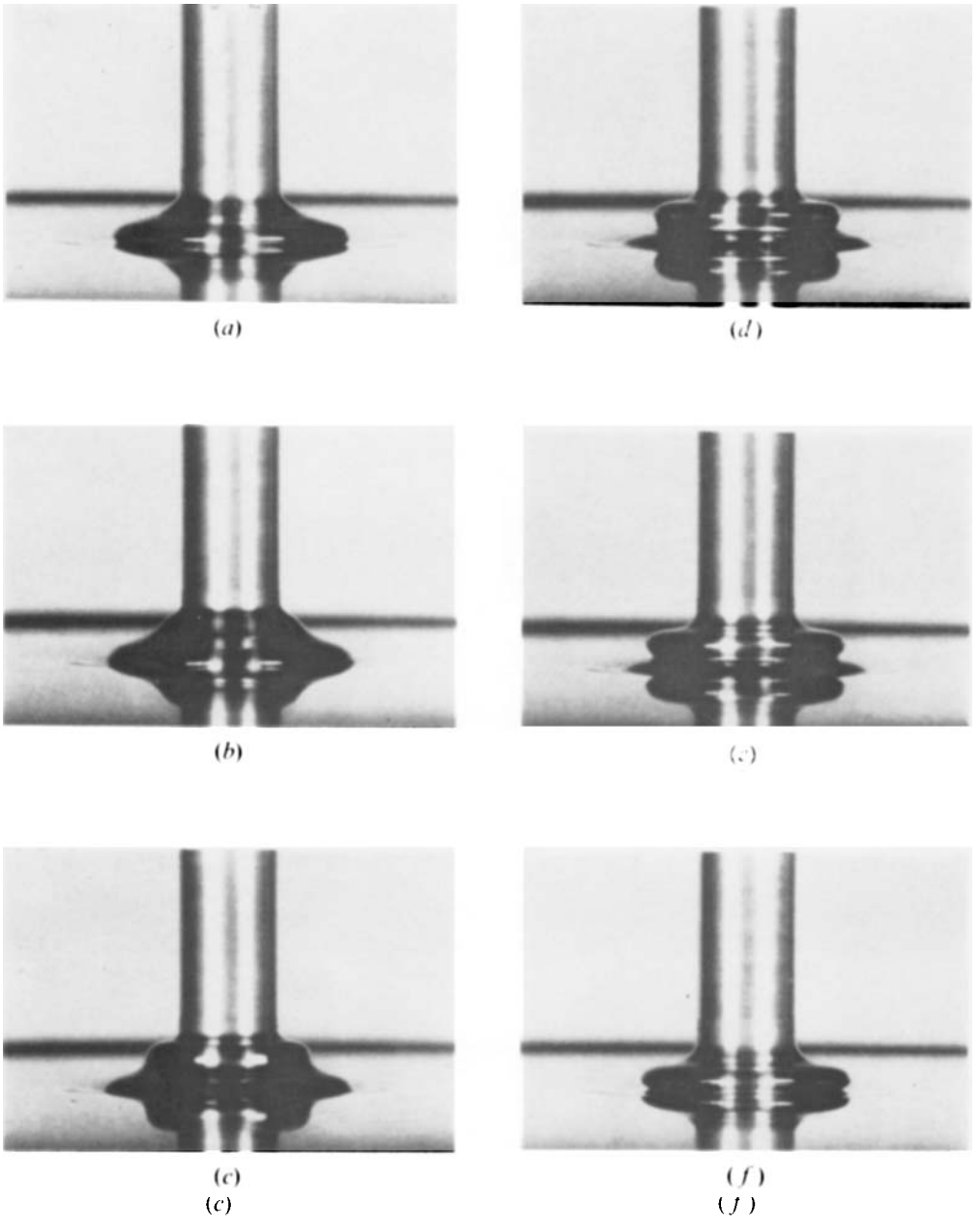

FIGURE 7. Time-periodic motion of the drop of climbing STP. Rod radius, 0·635 cm; rotational speed, 13·3 rov s^{-1}; frequency of periodic motion, 0·4 cycles s^{-1}.

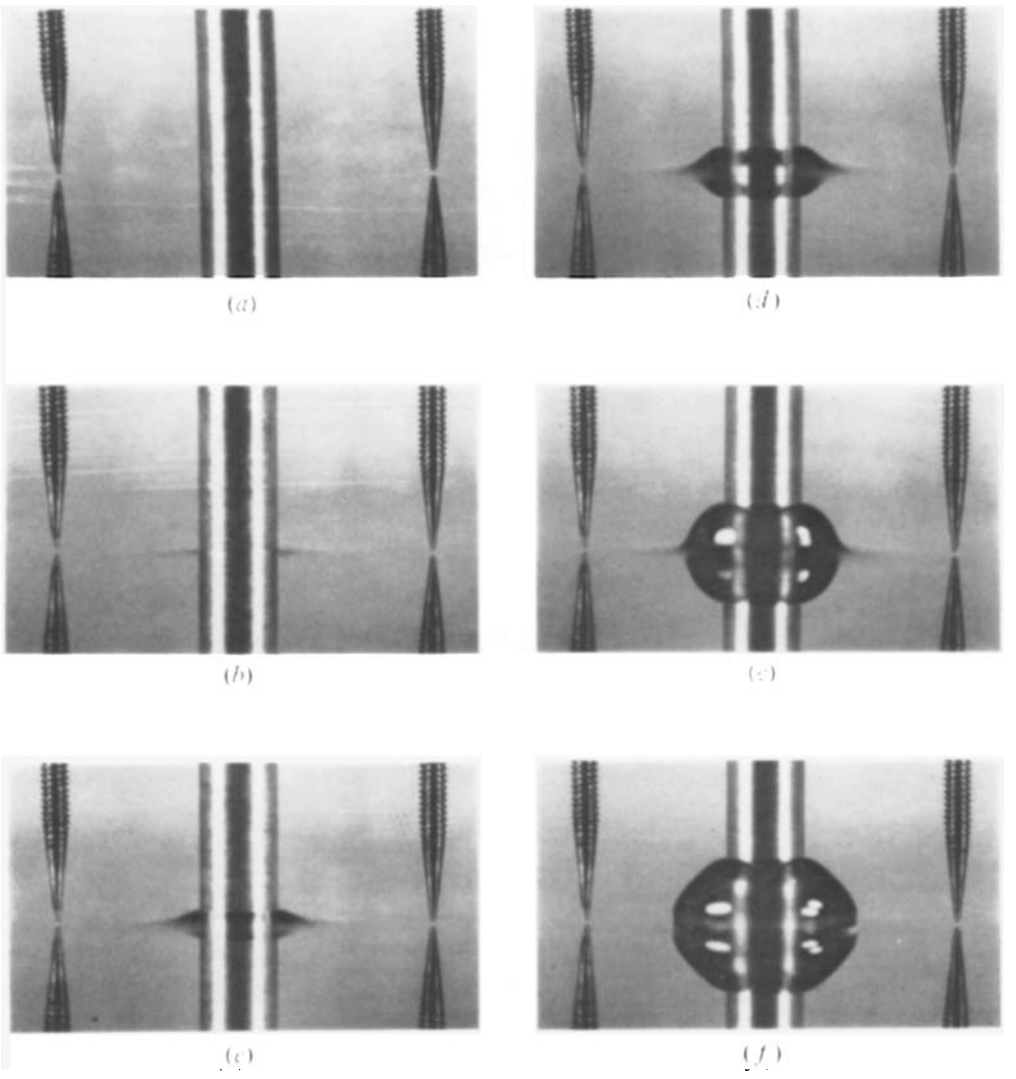

FIGURE 11. Change in shape of free surface of STP motor oil additive near a rod (radius $a = 0{\cdot}476$ cm), coated with Scotchgard, as rotational speed is increased; temperature 24·4 °C. (Apparent wavelike shape in (*d*)–(*f*) is an optical effect, arising from the lighting arrangement.)

	(*a*)	(*b*)	(*c*)	(*d*)	(*e*)	(*f*)
Speed (rev s^{-1})	0	1·0	2·2	3·0	5·0	7·0

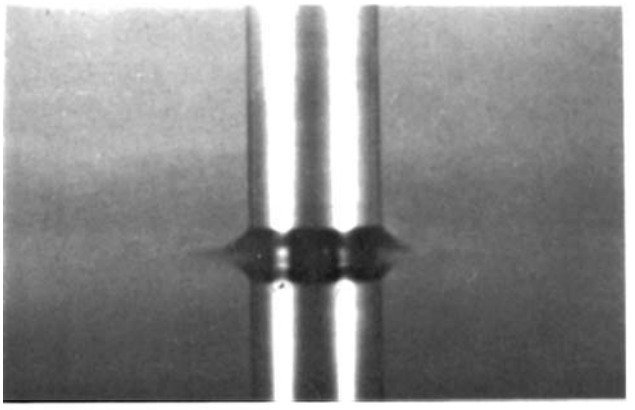

(*a*)

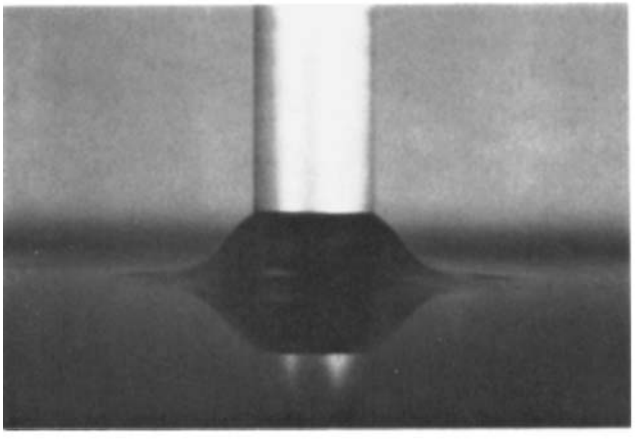

(*b*)

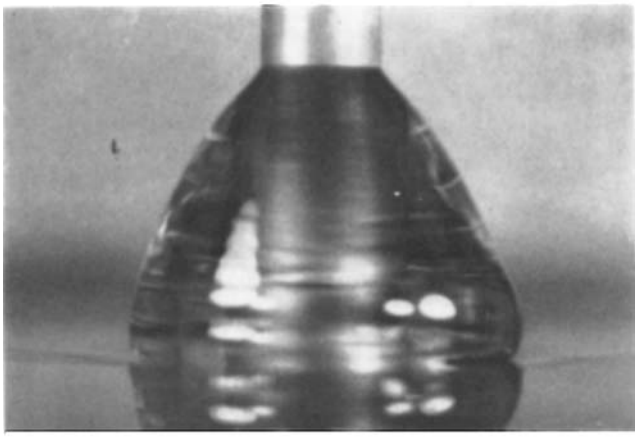

(*c*)

FIGURE 14. Influence of temperature on climb of STP near rod (radius $a = 0{\cdot}476$ cm), rotating at 5 rev s^{-1}.

	(*a*)	(*b*)	(*c*)
Temperature (°C)	46·1	25·6	5·0

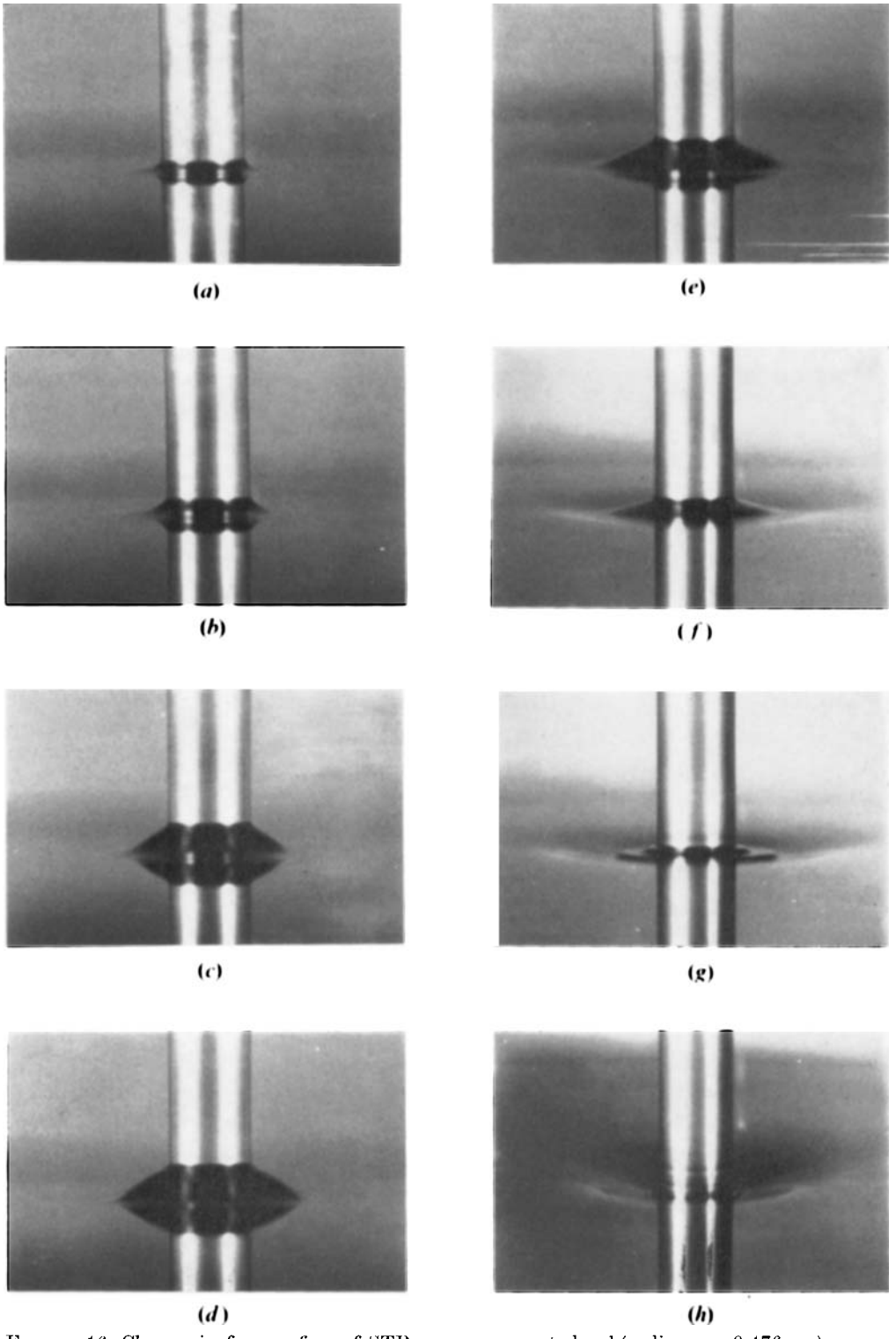

FIGURE 16. Change in free surface of STP near an uncoated rod (radius a = 0·476 cm), as rotational speed is increased; temperature, 46·1 °C.

	(*a*)	(*b*)	(*c*)	(*d*)	(*e*)	(*f*)	(*g*)	(*h*)
Speed (rev s^{-1})	0	5	10	15	23	30	37	50

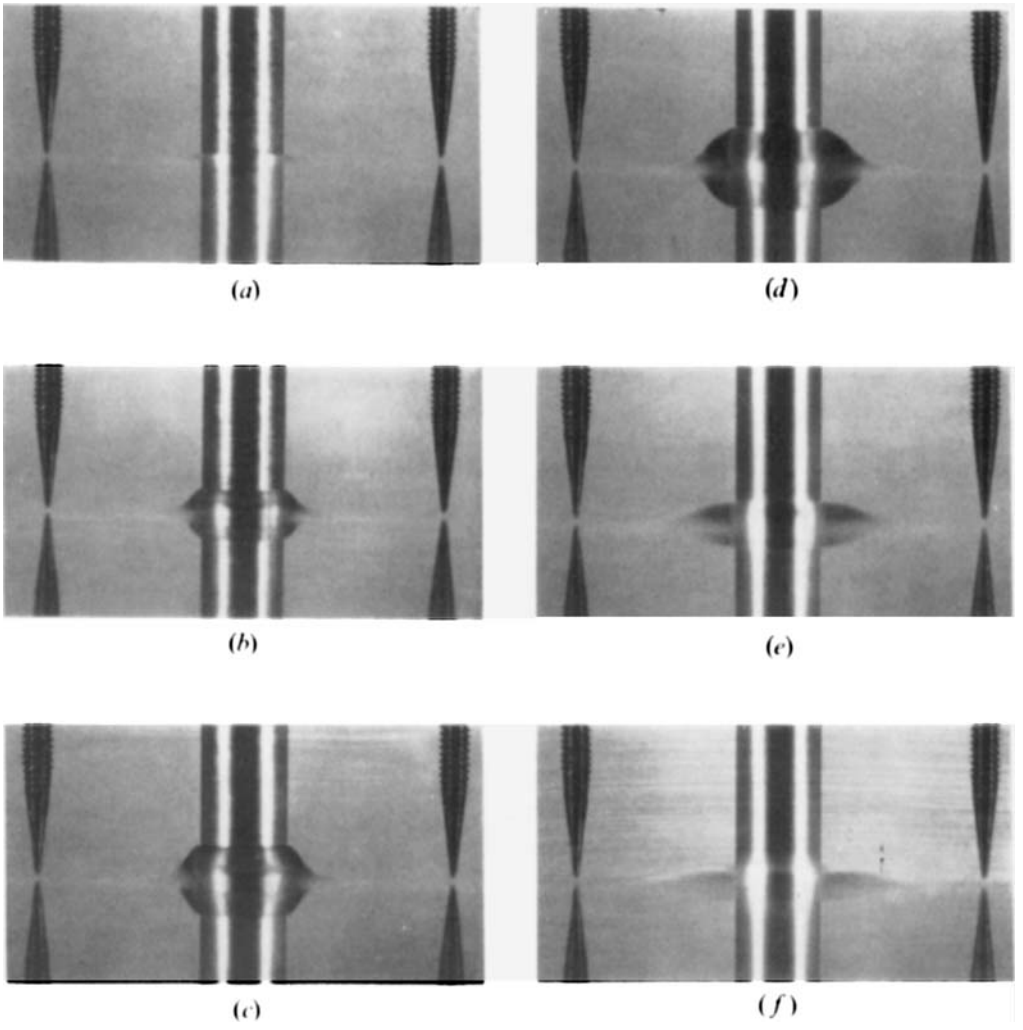

FIGURE 20. Change in free surface of polyacrylamide near a rod (radius $a = 0{\cdot}476$ cm) coated with Scotchgard, as rotational speed is increased; temperature, 38·3 °C.

	(*a*)	(*b*)	(*c*)	(*d*)	(*e*)	(*f*)
Speed (rev s^{-1})	1·0	2·5	5·5	25·0	45·0	70·0